Title: Titan mice are a unique bred mammalian model to study obesity and aspects of metabolic syndrome

Authors: Irene de-Diego[1†], Adrián Sanz-Moreno[2†], Annika Müller-Eigner[1†], Anuroop Venkateswaran Venkatasubramani[3], Martina Langhammer[4], Raffaele Gerlini[2,5], Birgit Rathkolb[2,5,6], Antonio Aguilar-Pimentel[2], Tanja Klein-Rodewald[2], Julia Calzada-Wack[2], Lore Becker[2], Axel Imhof[3], Chen Meng[7], Christina Ludwig[7], Franziska Koch[8], Angela Kuhla[9], Vanessa Caton[10], Julia Brenmoehl[10], Helmut Fuchs[2], Valerie Gailus-Durner[2], Andreas Hoeflich[10], Martin Hrabe de Angelis[2,5,11] and Shahaf Peleg[1*]

Affiliations:

[1]Research Group Epigenetics, Metabolism and Longevity, Leibniz Institute for Farm Animal Biology, 18196 Dummerstorf, Germany

[2]German Mouse Clinic, Institute of Experimental Genetics, Helmholtz Zentrum München, German Research Center for Environment and Health (GmbH), 85764 Neuherberg, Germany

[3]Department of Molecular Biology, Biomedical Center Munich, Ludwig-Maximilians University, Großhaderner Strasse 9, 82152 Planegg-Martinsried, Germany

[4] Institute Genetics and Biometry, Lab Animal Facility, Leibniz Institute for Farm Animal Biology, 18196 Dummerstorf, Germany

[5]German Center for Diabetes Research (DZD), 85764 Neuherberg, Germany

[6]Institute of Molecular Animal Breeding and Biotechnology, Gene Center, Ludwig-Maximilians-University Munich, Feodor-Lynen Str. 25, 81377 Munich, Germany

[7]Bavarian Center for Biomolecular Mass Spectrometry, Technical University of Munich, 85354, Freising, Germany

[8]Institute of Nutritional Physiology, Leibniz Institute for Farm Animal Biology, 18196 Dummerstorf, Germany

[9]Institute for Experimental Surgery, Rostock University Medical Center, Rostock, Germany

[10]Institute for Genome Biology, Leibniz Institute for Farm Animal Biology, 18196 Dummerstorf, Germany

[11]Chair of Experimental Genetics, TUM School of Life Sciences (SoLS), Technische Universität München, 85354 Freising, Germany

*Correspondence: shahafpeleg3@googlemail.com or peleg@fbn-dummerstorf.de

† These authors contributed equally.

Abstract

Obesity is a major culprit for metabolic syndrome (MetS). Relevant animal models can promote translational research on metabolic disorders. In this study, we suggest the Titan mouse as a new model for obesity and MetS. We show that adult Titan mice display several characteristics of MetS, including obesity and increased plasma levels of leptin, FGF21, insulin, cholesterol and triglycerides. This metabolic phenotype correlated with ectopic fat infiltration in the pancreas, 'whitening' of brown adipose tissue, increased inflammatory markers (IL-6, TNFα) and nodular thymic medullary hyperplasia. Liver transcriptomics and proteomics demonstrated alterations in lipid and sulfur metabolism, and in xenobiotic metabolic regulation. Interestingly, late dietary intervention in Titan mice reduced fat content, altered the expression of genes involved in lipid synthesis and cytochrome P450 detoxification, improved plasma health metrics and increased lifespan. Altogether, we propose the Titan mice as a powerful model for translational research and intervention on obesity and MetS.

Introduction

Obesity is seen as a major risk factor for metabolic syndrome (MetS). As MetS is especially prevalent in middle-aged people in the western world (*1–4*), targeting the onset and progression of MetS will promote health and benefit a large and growing part of the population. In humans, MetS is characterized by clustering three out of the five following criteria: high abdominal obesity, high blood sugar, high levels of fasting triglycerides, low levels of high-density lipoprotein (HDL) and elevated blood pressure. In commonly used MetS mouse models, these criteria may vary. For example, mouse models do not precisely mimic all aspects of human MetS, such as altered lipoprotein levels (high HDL in mice vs high LDL in human) (*5*). MetS in rodents may be partially defined by an obesity phenotype along with dyslipidemia, elevated glucose levels and/or hypertension, although the latter is inconsistent in obese mice (*5, 6*).

Despite differences in MetS manifestations between humans and mice, mouse models are essential to promote translational research and intervention on obesity and metabolic disorders. Common experimental rodent models of obesity and MetS usually involve high-fat diet (HFD), administration of drugs such as glucocorticoids and genetic intervention (*5, 6*). Genetic rodent models of obesity are based on the disruption of the leptin signaling pathways, including the mouse Leptin-deficient (ob/ob) and leptin receptor-deficient (db/db) or the rat Zucker Diabetic Fatty and DahlS.Z-Lepr^{fa}/Lepr^{fa} (DS/obese) model lines(*5–7*) These models display several but not all hallmarks of MetS(*6*)On the other hand, Koletsky rats that carry a nonsense mutation in the leptin receptor and POUND mice (C57BL/6NCrl-Lepr db-lb/Crl) display all conditions of MetS (*6*). A major disadvantage of these inbred and genetically impaired rodent models,

however, is that they do not reflect closely the human disease, thus rendering it difficult to translate findings in these rodents to human patients where notably leptin signaling is presumed to be intact. Therefore, there is a need for a model more closely resembling this multifactorial condition that is MetS. One approach to do so would be to use non-inbred rodent models not selected on genetic but on phenotypic traits relevant to obesity and MetS.

The Dummerstorf mouse line "Titan" (previously called 'DU6') is a result of a long breeding scheme that selected mice based on high body mass at 6 weeks of age. The initial population of mice was created in 1969/1970 by crossing four outbred (NMRI orig., Han/NMRI, CFW, CF1) and four inbred (CBA/Bln, AB/Bln, C57BL/Bln, XVII/Bln) populations (*8, 9*). As such, the Titan mice originated from a non-inbred population (*9*). The selection for high body mass started in 1975 with every generation constituted of 80 mating pairs (*10*) (except in two generations, see Methods). Throughout the selection process, an unselected population was maintained as a control group. As of 2020, after 45 years and over 180 generations of selection, this breeding scheme resulted in a short-lived, giant and obese mouse that weigh an average of 110 g, compared to 45 g for a non-selected mouse (*10–12*). Due to the uniquely long and successful breeding scheme, the apparent obesity of the mice potentially makes them a unique model to study the mechanisms underlying obesity, fat accumulation and MetS, and to allow possible interventions to reduce such metabolic disorders.

To characterize the phenotypic response of Titan mice to selection, several molecular studies have been conducted over time. For example, 6-week-old Titan mice from generation 80 (25 years ago) displayed high body mass, as

well as elevated levels of fat, insulin, leptin and growth hormone (*12*). A follow-up gene expression study in epididymal fat identified 77 differentially expressed genes (between control and Titan mice) involved, among others, in regulatory and metabolic pathways, and which might underlie the observed effect on body weight and fat accumulation (*13*). A more recent study showed that Titan mice (generation 146) displayed high blood glucose concentrations following an oral dose of 1 g/kg glucose at 6 weeks of age (*11*). Surprisingly, in older Titan animals, glucose tolerance progressively improved compared to unselected control mice (*11*).

In 2011/2012, the Titan mouse lines (generations 153 and 154) were transferred into a new state-of-the-art pathogen-free animal facility. Also, the mouse diet composition changed at that time point (*14*). These modifications might have impacted some characteristics of the Titan mice, calling for a thorough characterization of the present mouse line. More importantly, several key characteristics of the current Titan mouse, which might provide novel insights into their metabolic disorders, have not been evaluated yet. This includes full genomic sequencing, comprehensive histological analysis, lifespan characterization and various tissue omics (RNAseq transcriptome, proteome, epigenetic marks etc…).

We describe here a detailed evaluation of the present Titan mouse line, including the characterisation of histological, metabolic and transcriptional alterations that distinguish them from the unselected control mice. We hypothesized that, given their obese phenotype, the Titan mice might display several criteria of MetS and exhibit a shorter lifespan compared to control mice. We combined a phenotypic characterization of adult male mice around the time

point when the Titan population starts declining (4-5 months,10% death), together with RNA sequencing and proteome analyses. We also used the Titan mice to explore whether late dietary intervention may promote their lifespan. Our findings support the use of Titan mice as a suitable non-inbred mouse model to study the complexities inherent to obesity and MetS.

Results

Titan mice display increased size and reduced lifespan

We first characterized the phenotype of Titan mice with regards to body mass and lifespan – two traits known to be inversely correlated to each other (*15*). Current unselected control and Titan mice had an average weight of 35 and 90 g, respectively, at the age of selection (6 weeks) (Figure 1A). This marks a substantial weight gain for the Titan mice compared to that reported prior to 2013 (61.5 g at generation 80, 72 g at generation 146) (*12, 16*). Six-week-old Titan mice also displayed a considerably bigger size than control mice (Figure 1B). At 10–11 weeks of age, Titan mice reached 14.75 cm in body length (Figure 1C) and exhibited an increase in both total fat and lean mass (Figure 1D), as well as in fat percentage (Figure 1E). Fat distribution was also altered, with Titan mice accumulating as much as 4% intra-abdominal fat of total body weight compared to 1% in control mice (Figure 1F). These results confirm the obese phenotype of the Titan mice.

The lifespan of Titan mice was dramatically shorter than that of the unselected control strain (Log Rank test; $p<0.0001$, $\chi^2=124.9$) (Figure 1G). Under Standard Breeding Food (SBF), Titan mice reached 10% (pre-mortality plateau phase) and 50% death at 125 and 325 days respectively. Their average and maximal lifespan were 317.5 and 614 days respectively. The ages at 25%, 75% and 90% death, and the median lifespan are presented in Table S1. In comparison, control mice reached 10% and 50% death at 307 and 645 days respectively. Of note, at 17-19 weeks of age, when their survival reached the end of the pre-mortality plateau phase (10% death), Titan mice grew to an average of 110-115

grams (Figure 1H). Their body and skeleton were also substantially larger than those of controls (Figure 1I), making Titan mice one of the biggest laboratory mouse lines ever described.

Titan mice have altered fat characteristics and other signs of metabolic dysregulation

We next characterized Titan mice using the German Mouse Clinic (GMC) standardized phenotyping (Gailus-Durner et al., 2005, www.mouseclinic.de). Importantly, because Titan mice are not inbred, we increased the number of animals from 15 (standard GMC animal number per group and sex for inbred mice) to 20, focusing on one sex only (males), to avoid sex-specific confounding factors.

As cholesterol and fat are linked with obesity and MetS (*5*), we first sought to measure their plasma levels. We detected significantly higher fasting plasma levels of triglycerides, non-HDL and HDL cholesterol in Titan compared to control mice at 18-20 weeks of age (Figure 2A-C). Consistent with the notion that hyperlipidemia usually occurs in the presence of insulin resistance, insulin levels were more than 3-fold higher in ad libitum 16-17-week-old Titan mice (Figure 2D). Interestingly, however, glucose concentrations were similar in ad libitum-fed 16-17-week-old Titan and control mice (Figure 2E) whereas fasting glucose was elevated particularly in 10-11-week-old Titan mice (t-testing, p=0.057) (Figure S1). In addition, Glucose tolerance test in 13-14-week-old mice showed less efficient clearance in Titan mice (Figure S1).

Whitening of adipose tissue has been associated with obesity and obesity-related diseases (*17*). Indeed, at 16-17 weeks of age, when around 90% of the Titan mice were still alive (Figure 1G), Titan mice not only accumulated more intra-abdominal fat than controls (Figure 1F), but they also showed substantial whitening of brown adipose tissue (BAT), not observed in the BAT of control animals (Figure 2F).

Ectopic fat infiltration in the pancreas has been described as a marker of MetS(*18*) and was therefore investigated in Titan mice. At 16-17 weeks of age, Titan mice showed multifocal fatty cells in the pancreas, usually termed pancreatic lipomatosis or steatosis, without atrophic or inflammatory changes of the adjacent parenchyma, a phenotype not present in control mice (Figure 2G). We also found that the average levels of leptin, a hormone secreted by adipocytes(*3, 5, 19*) and known to modulate food intake and fat storage (*3, 5, 19*), were significantly higher (more than 5-fold; $P < 0.001$) in 16-17-week-old Titan mice compared to control mice (Figure 2H). Finally, we investigated whether the plasma concentration of fibroblast growth factor 21 (FGF21), a factor associated with MetS in humans (*20, 21*), was altered in Titan mice. At 16–17 weeks of age, Titan mice had elevated levels of FGF21 in the serum (Figure 2I), which further indicates metabolic alterations.

As obesity is linked to heart disease, we also assessed histological alterations in the heart of the Titan mice. Using Sirius Red staining, we detected fibrotic tissue in the hearts of three out of six 16-17-week-old and five out of six 24-26-week-old Titan mice (Figure S2).

Since hyperferritinemia is common in patients with MetS (*22*) or with liver dysfunction (*23*), plasma iron levels and iron binding capacity were measured in Titan mice. Titan mice displayed excess iron in plasma along with low unsaturated iron binding capacity (UIBC), resulting in reduced total iron binding capacity (TIBC) and increased transferrin saturation at 16-17 weeks of age (Figure S3).

Altogether, the combination of high fat content, dyslipidemia and reduced insulin sensitivity supports the existence of MetS in Titan mice (*1, 5*).

Titan mice display signs of systemic inflammation

Chronic inflammation markers are linked to obesity and MetS, as well as to aging and immune-related diseases (*24, 25*). To evaluate whether inflammation processes were altered in Titan mice, we first determined inflammation indicators in plasma of 16-17-week-old Titan mice. We found that the inflammatory cytokines interleukin 6 (IL-6) and tumour necrosis factor-alpha (TNFα) were significantly increased in the plasma of Titan mice compared to unselected control mice (Figure 3A and B). As an additional sign of inflammation, histological analysis of the thymus revealed the presence of nodular thymic medullary hyperplasia in Titan mice (Figure 3C). Immunohistochemistry of these medullar nodes revealed that they were composed mainly of B cells (Figure 3C).

Histological analyses revealed renal alterations in Titan mice

Obesity is a known risk factor for chronic kidney disease(*26, 27*). Indeed, our phenotyping has found renal alterations in three out of six 16-17-week-old and five out of six 24-26-week-old Titan mice. Kidney histological analyses revealed the presence of basophilic tubules, tubular casts and vessel thickening (Figure S4). Further, we observed elevated plasma electrolytes and mineral levels such as potassium, calcium, and inorganic phosphate, which might be due to impaired renal tubular function (Figure S5). In addition, plasma activity of alkaline phosphatase (ALP), a possible indicator of chronic kidney disease, as well as a marker of obesity (*28*), was increased in Titan mice (Figure 3D).

Titan mice display altered liver metabolism

We next evaluated possible alterations in liver function and metabolism of Titan mice. First, Alanine aminotransferase (ALAT) activity, a marker of liver damage (*29*), was significantly elevated in Titan mice at 16-17 weeks of age (Figure 3E). Combined Oil red O and Hematoxylin staining of the liver also revealed numerous small fat droplets in 16-17-week-old Titan mice (Figure 3F). No clear signs of hepatic steatosis were however found by H&E staining of 16-17-week-old Titan liver tissue (Figure S6).

Bilirubin, a waste product of heme metabolism in the liver, was significantly lower in 16-17-week-old Titan mice compared to controls (Figure 3G). In addition, plasma urea levels were lower in Titan than in control mice (Figure 3H), pointing to a possible dysregulation of protein metabolism and urea cycle

in the liver. Altogether, these findings suggest an altered liver metabolism in Titan compared to control mice.

Previous data support the notion that a high-fat diet and an increased body weight cause transcriptional alterations in the liver of mice (*30*). To identify the metabolic pathways possibly altered in the liver of Titan mice, we performed RNA sequencing on liver from 11-week-old and 19-21-week-old Titan and control mice. Principal component analysis (PCA) revealed distinct Titan and control transcriptomes (Figure 4A). Gene expression in younger and older controls also clustered together, but in Titan mice, the expression profile shifted between the age groups (Figure 4A).

Compared to age-matched controls, 11-week-old Titan mice exhibited 1150 upregulated and 1227 downregulated genes (Figure 4B, S7A and Table S3). The top 10 upregulated GO terms highlighted genes involved in several central metabolic processes such as fatty acid metabolism, lipid localization, nucleotide and coenzyme metabolism. Central metabolic regulators such as *mTOR, Elovl5, Elovl6*, and acetyl-CoA carboxylase were upregulated, suggesting altered fat metabolism in the liver (Figure 4C). The top 10 downregulated GO terms highlighted reduced xenobiotic, amino acid and sulfur metabolism (Figure 4C). For example, many genes from the cytochrome P450 family, including *Cyp2c37,* shown to be downregulated in high-fat diet (*30*), were downregulated in 11-week-old Titan mice (Figure 4C), which might indicate altered endogenous metabolite metabolism (*31*) or increased liver inflammation (*32,33*). Furthermore, several genes related to the methionine and folate cycle pathways [e.g., *Bhmt, Gnmt, Cth* (*Cgl*)*, Dmgdh*] were downregulated in Titan

mice (*30*). Taken together, liver transcriptomic analysis revealed several relevant metabolic alterations between Titan and control mice.

We next compared changes in gene expression between 11-week-old and 19-21-week-old mice. In the control mice (11 vs 19-21 weeks of age), few (52) differentially regulated genes were identified. In contrast, intragroup variability was significantly higher in Titan mice, making it possible to differentiate between the two groups (11 vs 19-21 weeks of age) in PCA analysis (Figure 4A). We identified 146 upregulated and 257 downregulated genes between 11-week-old and 19-21-week-old Titan mice (Figure S7B). We found no upregulated GO term composed of more than 10 genes. Nonetheless, the 19-21-week-old Titan mice had increased expression of several enzymes involved in glucose and insulin response compared to the 11-week-old Titan mice (See supplementary data). Also, *Cyp7b1*, which encodes an enzyme involved in cholesterol catabolism that converts cholesterol to bile acids and is upregulated in high-fat diet (*30*), was upregulated in 19-21-week-old Titan mice. On the other hand, the top 10 downregulated GO term highlighted genes involved in fatty acid, coenzyme and carbohydrate metabolism (Figure S7C).

The number of altered genes in 19-21-week-old groups (1521 differentially expressed genes compared to control) was lower than for 11-week-old groups (2377 genes) (Figure 4B and S7D). We found 693 upregulated genes and 828 downregulated genes in 19-21-week-old Titan mice. We observed a significant overlap of transcriptomic alterations between both age group comparisons, with 402 upregulated (out of 693) and 461 downregulated genes (out of 828). The top 10 GO terms at 19-21 weeks revealed the upregulation of genes involved in neuronal differentiation and peptidyl-tyrosine phosphorylation activity, thus

highlighting possible altered signal transduction and cellular signalling between Titan and control mice at 19-21 weeks of age (Figure 4D). Of note, we no longer observed a visible enrichment of genes involved in fatty acid metabolism in 19-21-week-old Titan mice compared to controls. The top 10 downregulated GO terms in 19-21-week-old Titan mice revealed genes involved in the regulation of xenobiotic, amino acid and sulfur metabolism (Figure 4D), similarly to the comparison at 11 weeks of age (Figure 4C). For example, respective to age-matched controls, both 11-week- and 19-21-week-old Titan mice had reduced expression of genes of the cytochrome P450 family compared to the respective control groups. On the other hand, genes involved in mitochondrial organization and mitochondrial respiration complex assembly were specifically downregulated in 19-21-week-old Titan mice, which may hint towards altered mitochondrial activity in older Titan mice.

To complement the transcriptome study, we compared the liver proteomes of Titan and control mice. As with the RNAseq data, larger proteomic changes were seen in the 11-week-old Titan to control comparison than in the 19-21-week-old comparison (Figure 5). Relative to age-matched controls, 11-weeks-old Titan mice exhibited 207 upregulated and 289 downregulated proteins, while 19-21-week-old Titan mice showed 125 upregulated and 142 downregulated proteins (Figure 5A and B, see choice of cut-offs in Methods).

Consistent with the transcriptome results, pathway enrichment analysis revealed increased fatty acid metabolism, lipid catabolism, and coenzyme metabolism while downregulation in xenobiotic, amino acid and sulfur metabolism in 11-week-old Titan mice (Figure 5C). In particular, fat utilization (enrichment of proteins such as ACACA, IDH1, and ACOX1) as well as lipid

biosynthesis (FASN, ACLY, and ACSL5) were enhanced, which might underlie the increased plasma cholesterol and triglyceride levels in these mice (Figure 2). Of note, we observed a substantial albeit incomplete overlap between factors identified in our transcriptomic and proteomic analyses (Figure S8), consistent with previous observations on these two techniques (*34*). The fact that many altered genes were not detected in the single-shot proteome analysis could be attributed to the lower relative coverage of the proteome approach (*34*).

Interestingly, proteins involved in lipid metabolism were also enriched in 19-21-week-old Titan mice compared to controls (Figure 5D), although this was not observed in the RNAseq top 10 GO terms (Figure 4D). We also found that proteins upregulated in 19-21-week-old Titan mice were associated with carbohydrate catabolism and coenzyme metabolism (Figure 5D), while downregulated proteins were enriched in amino acid and sulfur metabolism (Figure 5D), in line with the RNAseq analysis (Figure 4D). As with the transcriptome data, we observed a reduction in the abundance of BHMT, GNMT, and CTH (CGL), key proteins of the methionine cycle. Taken together, our proteome data support the notion that many alterations on the RNA level are also shown on the protein level, hinting towards increased fat metabolism.

Late dietary intervention at 12 weeks of age doubles the pre-mortality plateau phase in Titan mice

Dietary intervention, intermittent fasting or restriction of a specific macronutrient (i.e., proteins) is a well-studied and robust intervention to prevent or improve MetS

in humans (*35*) and to promote healthy lifespan in various animal models (*36–38*). However, not all mouse strains are responsive to caloric restriction (*39, 40*). Therefore, we investigated the impact of dietary restriction on the lifespan, fat accumulation and liver gene expression pattern of Titan mice.

To analyse the effect of a dietary intervention on Titan mice, we used a diet with moderate energy reduction (Energy Reduced Food, thereafter referred to as ERF, see Methods). Late ERF intervention at 12 weeks of age resulted in a weight reduction of 5–10% compared to the SBF-fed male siblings (Figure 6A MWU-test, P=0.0017). By 21 weeks, ERF-fed Titan mice had significantly reduced abdominal fat percentage compared to SBF-fed mice (Figure 6B; MWU-test, P=0.0313).

We next tested whether the ERF regime affected the expression level of liver genes that were already identified in our -omics experiments as significantly altered in Titan compared to control mice (Figures 4 and 5, See supplement list of genes). Interestingly, late ERF intervention reversed the expression profiles of some of the investigated genes. Notably, genes previously found to be downregulated in Titan versus control mice (e.g. *Dmdgh, Gnmt, Cth, Cyp2c37*) were upregulated in ERF-fed vs SBF-fed Titan mice (Figure 6C)(*30*). Similarly, genes previously found to be upregulated in Titan versus control mice (e.g. *Cyp7b1*) were downregulated in ERF-fed vs SBF-fed Titan mice (Figure 6C).

Time-restricted fasting can change and improve health metrics in human metabolic patients (*35*). Similarly, we show that the ERF regime lowered the levels of plasma cholesterol, HDL and glucose in Titan mice (Figure 6D)(*35*). Furthermore, leptin, glycerol and non-esterified fatty acids (NEFA) in the

plasma were decreased upon ERF regime (Figure 6D). Of note, obesity has been linked with higher levels of glycerol and NEFA (*41, 42*).

Finally, we investigated the impact of the ERF diet introduced at 12 weeks of age on the lifespan of Titan and control mice, compared to SBF-fed mice. The ERF diet significantly increased the lifespan of both Titan and control mice (Log Rank test; P=0.0087, χ^2=6.892 for Titan mice and P=0.0067, χ^2=7.360 for control mice) (Figure 6E). ERF-fed Titan mice reached the 10% and 50% death at 219 and 374 days, respectively, which is significantly longer than for the SBF-fed Titan mice (10% death at 125 days and 50% death at 325 days). In comparison, ERF-fed control mice reached 10% death at 377 days vs 307 days for SBF-fed control mice. The average lifespan of ERF-fed Titan mice was 359.5 days, compared to 317.4 days for SBF-fed Titan mice (Table S1).

Taken together, our results support the idea that a late ERF intervention causes physiological and transcriptional alterations coupled with an increase in lifespan in Titan mice.

Discussion

This study provides an in-depth phenotypic analysis of the giant Titan mouse line, with the aim to evaluate its possible use as a non-inbred model for obesity and metabolic syndrome (MetS).

The molecular phenotyping of the Titan mice showed several hallmarks of obesity and MetS, including a combination of increased body weight, high levels of fat in tissues, fasting triglycerides, fasting cholesterol and insulin (*5, 43*). In line with this, other mouse models of obesity, e.g. high-fat diet (HFD) mice or $Lep^{ob/ob}$ mice, revealed an elevation of several of these parameters(*44*) which supports the idea that Titan mice might represent a mouse model of obesity and MetS. In addition, our analysis revealed increased levels of FGF21, which is also a characteristic of obese mice and humans(*20*). Increased FGF21 might indicate FGF21 resistance(*45, 46*) which is potentially linked to obesity and the development of MetS (*21*). Titan mice also showed whitening of BAT, and ectopic fat in the pancreas, which are both linked to obesity and MetS (*17, 47*). Increased pancreatic fat might have implications for the onset of type 2 diabetes(*48*), which is frequently associated with insulin resistance. Accordingly, HFD mice showed increased pancreatic triacylglycerol content(*48*). Therefore, the observed alteration of the fatty acid millieu in the pancreas of Titan mice might contribute to islet dysfunction, in turn showing signs of insulin resistance. Furthermore, Titan mice showed early signs of heart fibrosis, which is also associated to obesity and hypertension, another hallmark of MetS (*49*).

In our study, Titan mice fed ad libitum showed higher fasting glucose levels at 10-11 weeks of age and increased insulin levels at 16-17 weeks of age. This

was surprising considering observations made on earlier Titan generations (*11, 12*). Previous Titan mice (generation 146) under chow diet had reduced fasting glucose levels compared to control at 7 weeks, and insulin levels significantly higher at 7 weeks but non-significantly higher at 16 weeks of age (*11, 12*). Moreover, our Titan mice showed impaired glucose clearance at 13-14 weeks of age, while Titan mice of generation 146 (under chow diet) showed a non-significant slower glucose clearance at 12 weeks of age (*11*). Possible causes for these differences are the further weight increase of Titan mice since generation 146, as well as the changes in diet and housing conditions implemented around generation 153 (*14*).

The Titan mice also exhibited several markers of systemic inflammation, such as high plasma levels of IL-6 and TNFα or thymic medullary hyperplasia, and of tissue (kidney, liver) damage, which may also be associated with obesity and MetS (*50–52*). Besides being associated to the initiation and progression of multiple diseases (*53, 54*), elevated circulating IL-6 and TNFα was also documented in obese mice and humans (*51, 55*) and in patients with MetS (*52*). Supporting this finding, several mouse models of obesity revealed increased accumulation of macrophages in the liver (*56, 57*) or in adipose tissue(*58*), indicative of increased inflammatory response in different tissues(*59*). It would be interesting to investigate, for instance using F4/80 antibody staining, whether macrophages also accumulate in various tissues of Titan mice. Nevertheless, obesity-induced systemic inflammation as indicated by enhanced circulating cytokine levels may lead to tissue damage. Also, ALAT is associated to tissue damage (*29*) and its plasma activity was significantly increased in Titan mice. Interestingly, ALAT (and aspartate aminotransferase –

ASAT) plasma level was also increased in a mouse model of obesity, after long-term exposure to HFD (*60*) .

Transcriptomic and proteomic changes in the liver of Titan mice were also identified, possibly reflecting metabolic alterations. At 11 weeks of age, genes involved in lipid metabolism and biosynthesis were consistently upregulated in Titan mice, which might account for the high levels of cholesterol and fasting triglycerides observed in this model. Of note, similar changes have been observed in the liver during MetS (*61, 62*). On the other hand, both 11-week- and 19-21-week-old Titan mice exhibited several downregulated genes and proteins associated with xenobiotic metabolism, such as cytochrome P450, indicating that Titan mice may have a generally reduced capacity to deal with toxic compounds in the liver. Xenobiotic metabolism strongly impacts the ability of the organism to maintain homeostasis and cope with disease, which may contribute to the increased morbidity of these mice (*63*). Also, Titan mice showed a reduced expression of genes related to the folate cycle and its downstream effectors, such as *Ahcy*, *Gsta* family and *Gnmt*. Such genes were already shown to be down-regulated in the mouse liver upon HFD (*30*). Taken together, our data suggest that Titan mice constitute a relevant model to study obesity and MetS and raise the possibility that targeting the expression levels of liver cytochrome P450 and methionine cycle enzymes might regulate obesity in Titan mice.

We describe – to the best of our knowledge for the first time – that Titan mice had a shorter lifespan than control mice and that their lifespan was increased under ERF feeding (from week 12 on). We also found that ERF-fed Titan mice had reduced intra-abdominal fat at 21 weeks and that ERF feeding partially

reversed the expression pattern of metabolic gene expression in the liver, including key metabolic enzymes such as *Cyp7b1* and *Cyp2c37,* or of enzymes of the methionine cycle such as *Cth*, *Gnmt*, and *Dmdgh* (*30*). Several of these genes have already been implicated in mediating the benefits of caloric restriction (*64–66*). For example, recent work showed that CTH (CGL) mediates the dietary restriction response via H_2S production (*65*). Similarly, food intake restriction increases GNMT levels, promotes energy homeostasis, and increases healthy lifespan (*66, 67*). Furthermore, late ERF regime is sufficient to improve several health metrics in the Titan mice, similarly to time-restricted eating in metabolic syndrome patients, which highlight the relevance of Titan mice as model to study obesity, metabolic syndrome and associated interventions to treat them (*35*).

We propose that the Titan mice represent a novel mouse model for studying MetS, with several advantages over other currently used mouse models. First, no genetic alterations are needed to achieve the obesity phenotype in Titan mice. For example, unlike commonly used MetS mouse models, Titan mice have intact leptin signalling (*5*). Also, in contrast to $Lep^{ob/ob}$ mice that possess poor fertility (*5*), Titan mice are relatively easy to maintain and can provide sufficiently large populations to conduct various studies. Also, they stem from a more diverse genetic population than classical inbred mice and therefore studying MetS in Titan mice may be more relevant to human population studies. Indeed, the phenotype of the Titan mice is a possible consequence of several genetic and epigenetic changes, thus better reflecting the situation in humans. In that regard, it would be informative to obtain full sequencing of the mice and

to study the phenotype of hybrids resulting from a cross of Titan and unselected mice.

Importantly, no diet alterations are needed to achieve the obesity phenotype in Titan mice. This offers the opportunity to study the impact of diet intervention on their obesity and metabolic phenotypes. Another apparent advantage in this regard is that the Titan population starts declining at a young age (4-6 months), and thus testing interventions allows yielding rapid results. For example, the apparent benefit in lifespan of our ERF intervention was obtained in 21-week-old Titan mice, whereas the same intervention usually takes much longer in other mouse models (*39*).

In conclusion, the Titan mouse line represents a remarkable scientific achievement in breeding of mice. The detailed phenotypic analysis described here strongly supports the Titan line as a relevant model to study obesity and MetS. Importantly, as non-inbred mice, Titan animals may better reproduce the genetic variability of human populations and thus might be a useful option for preclinical drug testing (*39*). The present phenotypic analysis provides a strong basis for the characterization of the Titan model as a novel tool for studying and potentially developing pharmaceutical interventions targeting obesity and metabolic disorders.

Acknowledgments

We would like to thank our technician Verena Hofer-Pretz for performing many of the experiments for this study, as well as managing the laboratory conditions that enabled this work. The authors thank Ines Müntzel, Karin Ullerich, Sabine Maibohm, Benita Lucht, Hildburg Meier from the mouse facility for the animal care and technical assistance. The authors also thank Erika Wytrwat for technical support. The GMC would like to thank the technicians and animal care takers involved in this project for their expert technical help. We also thank Franziska Hackbarth, Nina Lomp and Hermine Kienberger for their excellent laboratory assistance at the BayBioMS. The authors thank Dr. Anne Rascle of AR Medical Writing (Regensburg, Germany) for providing medical writing and editing support. The authors also thank Dario Riccardo Valenzano and Christoph Anacker for their comments on the manuscript.

The study was supported by the Leibnitz society and by the German Federal Ministry of Education and Research (Infrafrontier grant 01KX1012 to MHdA); German Center for Diabetes Research (DZD) (MHdA), the Helmholtz Alliance ‘Aging and Metabolic Programming, AMPro` (RG).

Author contributions

SP conceptualized the project. ML prepared all the mice work, conducted the survival curves with the weight measurements and assisted with conceptualizing this work. ML also maintains the Dummerstorf selection line. AH contributed to this work by the management of pilot studies on life

expectancy in the mouse model used in this study. ID-D and AV-V prepared the RNAseq. AM-E prepared the proteome data. AS-M, RG, BR, AA-P, TK-R, JC-W performed mouse phenotyping tests and analyzed the data, LB supported data analyzes and manuscript preparation, CS coordinated and VG-D, HF and MHdA supervised the project at the GMC and conceived phenotyping test pipeline. AV-V analyzed the RNA-seq and generated the data visualization. AI supervised AV-V's work. CM and CL ran, analyzed and visualized the proteome data. FK isolated the blood for the ERF experiments. VC ad JB prepared and analyzed the Oil red O/ hematoxylin straining. ID-D, FC, AK and SP wrote the initial manuscript. All authors contributed to the final version of the manuscript. AM-E generated all the final figures for the paper.

Declaration of interests

Authors declare no competing interests.

Figure legends

Figure 1. Titan mice, a product of 180 generations of selection, is a giant short-lived mouse strain.

(A) Average weight (g) of 6-weeks-old control (blue) and Titan (red) male mice over 180 generations. Generations were composed of roughly 80 pairs of mice, unless stated otherwise (see Methods). Dotted line indicates new mouse housing (see Methods). (B) Representative images of unselected control mice (left) and selected Titan mice (right) at 6 weeks, at the time of the selection. (C) Body length (cm) of 10–11-week-old Titan mice compared to age-matched control mice. Control (n = 20) and Titan (n = 17) mice (D) Total fat and lean mass of control (n = 20) and Titan (n = 17) mice at 10–11-week-old. (E) Total percentage of fat in control (n = 20) and Titan (n = 17) mice. (F) Percentage of intra-abdominal fat (n = 10 per group) at 10–11-week-old. (G) Comparison of lifespans and mortality rates of Titan and control male mice showing significant reduced life span of Titan mice (Log Rank test; $p < 0.0001$, $\chi^2=124.9$). Titan mice reached the end of the pre-mortality plateau phase at 17-18 weeks of age (10% death). (H) After the first 16-19 weeks of life, Titan mice reached 110–115 g, whereas average control animals weighed 45 g. (I). Representative X-ray images of control and Titan mice at 16-17 weeks of age. Control (n = 38) and Titan (n = 31) mice. ***$P < 0.001$. Error bars indicate SEMs. Unpaired two-tailed *t*-tests with Welch's correction were used to calculate *P*-values.

Figure 2. Titan mice display several molecular criteria for obesity and metabolic syndrome.

(A-C) Plasma analyses comparing control and Titan mice after fasting at 18–20 weeks. Titan mice showed higher levels of triglycerides (p = 0.0055) and both non-HDL (p = 0.0022) and HDL cholesterol (n= 20 control vs 19 Titan). (D) Insulin levels in control (n = 19) and Titan (n = 18) mice at 16–17 weeks of age. (E) Plasma glucose levels in control (n = 20) and Titan (n = 17) mice at 16–17 weeks of age (p = 0.789). (F) Representative images of hematoxylin and eosin (H&E)-stained brown adipose tissue (BAT) from control (n = 6) and Titan (n = 5) mice (20x magnification) at 16–17 weeks of age. (G) Representative images of H&E-stained pancreas from control (n = 6) and Titan (n = 6) mice (2.5x magnification) at 16–17 weeks of age. (H) Leptin levels in control (n = 20) and Titan (n = 18) mice and (I) Significantly higher FGF21 levels in the Titan mice line compared to the control mice line (N=20 control vs 18 Titan) (**$P < 0.01$ ***$P < 0.001$. Error bars indicate SEMs. Unpaired two-tailed *t*-tests with Welch's correction were used to calculate *P*-values.

Figure 3. Titan mice show early signs of increased inflammation and altered liver metabolism.

Comparison of Titan and control mice at 16–17 weeks of age. (A and B) IL-6 plasma levels (p = 0.0086) in control (n = 13) and Titan (n = 17) mice, and TNFα plasma levels in control (n = 20) and Titan (n = 18) mice. (C) Representative images of hematoxylin and eosin (H&E) staining and B-cell immunohistochemistry (IHC) of the thymus of control (left) and Titan (right) mice (2.5x magnification). IHC of thymic medullar nodes revealed that they are composed mainly of B-cells (CD45R/B220-positive) instead of T-cells (CD3-

positive). Images in squares were taken at 10x magnification (n = 4–6 per group). (D and E) Alkaline phosphatase (ALP) (p = 0.0019) and alanine aminotransferase (ALAT) (p = 0.0262) levels in control (n = 20) and Titan mice (n = 18). (F) Oil Red O with Hematoxylin of fat in liver of control and Titan mice (n = 4 per group) (G) Bilirubin levels in control (n = 20) and Titan mice (n = 18) (p = 0.0019). (H) Urea levels of control (n = 20) and Titan (n = 18) mice (p = 0.0132). *$P < 0.05$, **$P < 0.01$ ***$P < 0.001$. Error bars indicate SEMs. Unpaired two-tailed *t*-tests with Welch's correction were used to calculate *P*-values.

Figure 4. Liver transcriptome analyses reveal differential expression of genes associated with metabolic pathways in Titan mice.

(A) Principal component analysis (PCA) of liver transcriptomes revealed clustering differences between Titan mice and controls. Control mice at 11 weeks and 19-21 weeks had similar transcriptomes, while younger and older Titan mice had distinct transcriptomes. (B) Heat map showing significantly altered genes in control and Titan mice at 11 weeks and 19-21 weeks of age. (C) GO term analysis in 11-week-old Titan mice (compared with corresponding control) had upregulated fatty acid metabolism, various lipid catabolism, nucleotide and coenzyme metabolism whereas downregulated pathways highlighted reduced xenobiotic, amino acid and sulfur metabolism. (D) GO term analysis revealed no upregulated pathways composed of more than 10 genes in 19-21-week-old Titan mice. Top 10 downregulated pathways highlighted a reduction in fatty acid, coenzyme and carbohydrate metabolism, as well as response to wound healing. (n = 5 per group).

Figure 5. Liver proteome analyses reveal differences in metabolic protein levels between control and Titan mice.

(A) Heat map comparing proteomes of 11-week-old control and Titan mice. (B) Heat map comparing proteomes of 19-21-week-old control and Titan mice. (C) GO term analysis of 11-week-old mice indicated increased fatty acid metabolism, various lipid catabolism, and coenzyme metabolism while downregulation in xenobiotic, amino acid and sulfur metabolism. (D) GO term analysis of 19-21-week-old mice showed upregulation of proteins involved in fatty acid metabolism, carbohydrate catabolism and coenzyme metabolism and downregulation of proteins involved in amino acid and sulfur metabolism (n = 6 per group).

Figure 6. Late intervention by switching to energy-reduced food (ERF) doubles the pre-mortality plateau phase in Titan mice.

(A) Switching standard feeding (SBF) to ERF at 12 weeks resulted in a persistent average weight loss in Titan siblings. At 21 weeks of age, ERF-fed Titan mice were 10% lighter in weight than SBF siblings (n = 23 per group). MWU-test, P=0.0017 (B) Compared to age-matched control Titan mice, ERF-fed Titan mice had a lower percentage of intra-abdominal fat at 21 weeks (n= 7 per group). Paired MWU-test, p = 0.0313. (C) RT-qPCR comparing gene expression of candidate genes (from Figure 4) of ERF- and control-fed Titan mice siblings at 21 weeks of age (n = 7 per group). Paired t-test was performed followed by multiple correction to calculate P-values pval.adj (*Dmdg*)=0.032,

(*Gnmt*)=0.012, (*Bhmt*)=0.736, (*Cyp7b1*)=0.008, (*Elovl5*)=0.736, (*Cyp2c37*)=0.012, (*Acaca*)=0.0587, (*Cth*)=0.012. (D) Late ERF feeding at 12 weeks of age decreased the levels of plasma cholesterol (pval.adj=0.00013), HDL (pval.adj=0.0013), Glucose (pval.adj=0.043), Leptin (pval.adj=0.043), Glycerol (pval.adj=0.0165) and NEFA (pval.adj=0.00132) in 21 weeks old mice. (n= 10 per group). MWU-test, by multiple correction to calculate P-values (E) Switching to ERF feeding at 12 weeks of age (vertical dashed line) increased the lifespan of both the Titan and control mice (Log Rank test; p=0.006, $\chi 2$=7.542 for Titan mice and p=0.0412, $\chi 2$=4.166 for control mice). ERF-fed Titan mice reached the 10% and 50% death at 219 and 374 days respectively which is significantly longer that the SBF-fed Titan mice (10% death = 125 days and 50% death = 325 days). The average and maximal lifespan of ERF-fed Titan mice were 359.5 and 660 days respectively. ERF-fed control mice reached 10% death at 377 days vs 307 days for SBF-fed control mice. The ages at 25%, 75% and 90% death, and the median lifespan are presented in Table S1. *P < 0.05, **P < 0.01, ***P < 0.01. Error bars indicate SEMs.

Materials and Methods

Animals and housing conditions

All procedures were performed in accordance to national and international guidelines and approved by our own institutional board (Animal Protection Board from the Leibniz Institute for Farm Animal Biology). At the German Mouse Clinic, mice were maintained in IVC cages with water and standard mouse chow according to the directive 2010/63/EU, German laws and GMC housing conditions (www.mouseclinic.de). All tests were approved by the responsible authority of the district government of Upper Bavaria.

At the FBN, the animals were maintained in a specific pathogen-free (SPF) environment with defined hygienic conditions at a temperature of 22.5±0.2°C, at least 40% humidity and a controlled light regime with a 12:12-h light-dark cycle. The mice were kept in Polysulfon-cages of 365 x 207 x 140 mm (H-Temp PSU, Type II L, Eurostandard, Tecniplast, Germany) and had free access to pellet concentrate and water. Mice were fed ad libitum using a standard breeding food (SBF) including 22% crude protein, 34% starch, 5% sugar, 4.5% crude fat, 3.9% crude fiber and 51.2% N free extracts (ssniff® M-Z autoclavable, Soest, Germany).

For the energy-reduced survival experiment, the mice were fed with a mouse maintenance energy-reduced diet (ERF) characterized by a low energy density and high fiber contents (15% crude protein, 21% starch, 5% sugar, 3.1% crude fat, 14.2% crude fiber and 48.8% N free extracts (ssniff® M-H autoclavable, Soest, Germany). Mice were place under the ERF diet starting at 12 weeks of age.

In both control and Titan lines, the litter size was standardized to 10 (5 male / 5 female pubs) immediately after birth and until weaning occurs at an age of 21 days. Starting with an age of three weeks, males of different litters were grouped in a cage at three animals per cage. The first survival experiment was done with n=104 Titan males from generation 181 and n=96 control males originating from generation 192. The second survival experiment under the ERF diet started with n=103 Titan and n=102 control males, one generation later. Additionally, 27 Titan male full siblings pairs of generation 183 were divided into two contemporaneous groups and were fed with SBF or ERF after 12 weeks of age, to generate the samples to analyze metabolic parameters. Individual weights of all animals were taken regularly each three weeks starting with an age of 21 days.

During the survival experiments, all included males were observed daily for their health condition. If physical impairments were detected which would cause considerable suffering or substantial pain to the animals they were sacrificed and such incidents were documented accordingly.

Origins of the growth selected strain and the control strain.

We used mice of an unselected strain (FZTDU) as control and a strain selected for high body mass at day 42 of age (DU6/Titan), both bred at the Leibniz Institute of Farm Animal Biology (FBN), Dummerstorf, Germany.

The initial population of mice was created in 1969/1970 by crossing four outbred (NMRI orig., Han/NMRI, CFW, CF1) and four inbred (CBA/Bln, AB/Bln, C57BL/Bln, XVII/Bln) populations(*8*). Mice of the control line FZTDU used in

this experiment were mated randomly over about 192 generations with a population size of 100 to 200 mating pairs per generation, respectively. Four generations of the control line are generated yearly using a rotation procedure of Poiley (1960) to avoid inbreeding(*68*).

The growth selection started in 1975 thus creating the Dummerstorf growth line DU6 (Titan) by selection for high body mass by sib selection (Bünger et al., 2001) in a conventional environment. In every generation, 80 mating pairs were made at an age of 63 ± 3 days(*10*). The selection procedure as described above was maintained for 153 generations. Only seven males and seven females of the DU6 line belonging to generation 153 and 154, respectively, were used as new founder animals after embryo transfer in a new built animal facility. Additionally, the health status was changed after 2011-2012 when the mouse lines were transferred into a new animal facility with specific pathogen-free environment conditions. Over the entire term of the following five generations the new breeding population of at least 60 pairs of Titan DU6 mice were established, taking care of an equal distribution of all genes of the 14 founder animals. In opposition to the former sib selection in generation number 161, breeding value estimation started introducing a two-trait BLUP (**B**est Linear **U**nbiased **P**rediction) animal model for male and female body mass. The raising inbreeding coefficient in the selection line was then controlled by the 'Optimal Genetic Contributions to the Next Generations' method of Meuwissen(*69*).

Histology, plasma, DEXA – GMC

Two cohorts of 20 DU6/Titan and 20 control (FZTDU) male mice were subjected to an extensive phenotypic screening at the German Mouse Clinic (GMC), including standardized phenotyping in e.g. the areas of energy metabolism, clinical chemistry, pathology(*70*) (see also www.mouseclinic.de). The phenotypic tests were part of the GMC screen and were performed according to standardized protocols as described before(*71–73*). Variations in protocols are specified. Depending on the test performed, animal number varied, as indicated in the respective Figure/Table.

Plasma clinical chemistry analyses included determination of blood lipid and glucose levels on freshly collected Li-heparin-plasma samples collected after overnight food withdrawal and measurement of a broad spectrum of parameters including ALAT, ASAT and ALP activity, urea and bilirubin levels in samples collected in ad libitum fed state during final blood withdrawal. Analyses wer performed using an AU480 clinical chemistry analyser (Beckman-Coulter, Germany) as described previously (Rathkolb et al. 2013a, 2013b). Samples collected during final blood withdrawal were frozen and stored at -80°C until the day of analysis.

Glucose-Tolerance-Test (GTT)

GTTs were performed afer a 6-hours-lasting food withdrawal. Before food withdrawal and in the beginning of the test, the body weight of mice was determined. For the determination of the fasting blood glucose level a small drop of blood collected from the tail tip was analyzed with the Accu-Chek Aviva glucose analyzer (Roche/Mannheim). Thereafter, mice were injected

intraperitoneally with 2 g of glucose per kilogram of body weight using a 20% glucose solution, a 25-gauge needle, and a 1-ml syringe. Fifteen, 30, 60, and 120 min after glucose injection, additional blood samples (one drop each) were collected and used to determine blood glucose levels as described before. Repeated bleeding was induced by removing the clot from the first incision and massaging the tail of the mouse. After the experiment was finished, mice were placed in a cage with plentiful supply of water and food.

The determination of the IL-6, TNFα, Insulin, leptin and FGF21 plasma levels was performed with a combined electrochemiluminescence multiplexed assay system (Meso Scale Discovery, MSD, Rockville, MD USA).

X-ray imaging was performed in an UltraFocus DXA system (Faxitron Bioptics, LLC) with automatic exposure control.

Macroscopic examination was performed in combination with histopathological analyses using hematoxylin and eosin (H&E) staining on formalin-fixed paraffin-embedded sections (3 μm) of tissues from 29 organs as described in www.mouseclinic.de/screens/pathology. Immunohistochemistry was carried out in a Leica Bond III (Leica Biosystems) automatic stainer. Heat-induced antigen retrieval was performed with citrate buffer (pH 6) for 30 minutes (AR9961; Bond TM Epitope Retrieval Solution; Leica Bio systems) in 2-μm-thick sections. For the identification of specific cells in the thymus, antibodies against CD3 (Clone SP7; ZYT-RBG024; Zytomed systems) and CD45R/B220 (Clone RA3-6B2; 550286; BD Pharmingen) were employed and the staining was detected with DAB chromogen. The slides were scanned using a

Hamamatsu NanoZoomer 2.0HT digital scanner and analysed by two independent pathologists using NDP.view2 software (Hamamatsu Photonics).

Staining of triglycerides in liver tissues

Liver tissue samples embedded in Tissue Tek (Weckert, Kitzingen, Germany) were cryosectioned (8 µm thick) using a Leica CM3050 S (Leica, Bensheim, Germany) cryostat microtome. After fixation in 4% paraformaldehyde / PBS for 1 min at RT, the slides were stained in RedOil solution (1 mg/ml RedOil (#A12989, Alfa Aesar, Karlsruhe, Germany) in 60% Isopropanol) for 10 min and then washed three times in distilled water. The slides were further stained in hematoxylin for 5 minutes and washed for 3 min in fresh tap water before with Aquatex (Roth, Germany) and dried overnight. The staining of the triglycerides was visualized with a Nikon Microphot-Fxa microscope (Nikon Instruments Europe B.V., The Netherlands) and an image analysis system (Nikon Digital Sight, DS-L2).

RNAseq

For RNA extraction and library preparation, 50 mg of tissues (liver) were homogenized in Trizol (Thermo Fisher; cat. no. 15596026) and processed according to the manufacturer's instructions. RNA concentration and $A_{260/280}$ ratio was measured with NanoDrop, followed by Bioanalyzer using RNA pico assay kit using manufacturer's protocol. rRNA depletion was performed using NEBNext rRNA Depletion Kit (Human/Mouse/Rat) [NEB #E6310] and library preparation for RNA-sequencing was performed using NEBNext Ultra II

Directional RNA Library Prep Kit for Illumina [NEB #E7760] following manufacturer's protocol.

For RNA-seq data analysis, read mapping of mouse tissue samples to the mouse genome (GRCm38) and counting of reads mapped to genes were performed using STAR v2.5.3a (*74*) using parameters --quantMode GeneCounts and providing annotation –sjdbGTFfile Mus_musculus.GRCm38.97.gtf. Aligned reads were filtered for unmapped, multimapped and ambiguous reads. Reads from histones and Y chromosome were removed. Reads were also filtered if they had low read counts in at least two samples. Differential expression analysis was carried out using DESeq2 v1.24.0 (*75*) at an adjusted p-value cut-off of 0.05. GO term analysis was performed using ClusterProfiler v3.12.0 (*76*) at a FDR of 0.05 using Benjamini-Hochberg procedure and with a log fold change cut-off of 0.5. GO terms containing at least a minimum of 10 genes were considered.

All the plots generated for RNA sequencing data were obtained using ggplot2 v3.2.1 (*77*) unless otherwise stated. For heatmaps and Venn diagram for RNA sequencing and proteomics data, pheatmap v1.0.12 (Kolde, R. (2013). pheatmap: Pretty Heatmaps. R package version 0.7.7. http://CRAN.R-project.org/package=pheatmap) and VennDiagram v1.6.20 (*78*) were used respectively with genes (or proteins) passing the adjusted p-value significance of 0.05.

Proteomics

The proteome protocol was adopted from(*79, 80*) with the following modifications. A total of 200 mg of frozen mice liver was homogenized in 500 µl lysis buffer [50 mM Tris-HCl pH 7.5, 500 mM NaCl, 1 ml EDTA, 0.1% NP-40 and 20% glycerol, 15 mM sodium butyrate, 60 mM of sirtinol and one protease inhibitor tablet (Roche)] and then supplemented with 200 µl 6 M urea/2 M thiourea and 900 µl lysis buffer. To reduce disulfide bonds, samples were treated with 1 mM DTT for 45 min at 4°C, followed by a treatment with 550 mM IAA for 30min at 4°C in the dark. 1 M ammonium bicarbonate (Ambic) was added to the samples to get a final concentration of 1 M urea. The proteins were digested for 5 hours with Lys-C (Wako) at room temperature and overnight with trypsin (Worthington). Samples were acidified and diluted with TFA to a final concentration of 1% TFA before being loaded on the Sep-Pak Light C18 cartridges (Waters). Columns were washed with 0.1% TFA and eluted with 60% acetonitrile (ACN)/0.25% TFA. The eluates were dried out by speed vacuum. The pellets were re-dissolved in buffer [50 mM Hepes pH 8.0 and 50 mM NaCl] and the protein concentration was measured by Nanodrop.

LC-MS/MS measurements were performed on an Ultimate 3000 RSLCnano system coupled to a Q-Exactive HF-X mass spectrometer (ThermoFisher Scientific). For full proteome analyses ~0.25 µg of peptides were delivered to a trap column (ReproSil-pur C18-AQ, 5 µm, Dr. Maisch, 20 mm × 75 µm, self-packed) at a flow rate of 5 µL/min in 100% solvent A (0.1% formic acid in HPLC grade water). After 10 minutes of loading, peptides were transferred to an analytical column (ReproSil Gold C18-AQ, 3 µm, Dr. Maisch, 450 mm × 75 µm, self-packed) and separated using a 110 min gradient from 4% to 32% of solvent B (0.1% formic acid in acetonitrile and 5% (v/v) DMSO) at 300 nL/min flow rate.

Both nanoLC solvents (solvent A = 0.1% formic acid in HPLC grade water and 5% (v/v) DMSO) contained 5% DMSO to boost MS intensity.

The Q-Exactive HF-X mass spectrometer was operated in data-dependent acquisition (DDA) and positive ionization mode. MS1 spectra (360–1300 m/z) were recorded at a resolution of 60,000 using an automatic gain control (AGC) target value of 3e6 and maximum injection time (maxIT) of 45 msec. Up to 18 peptide precursors were selected for fragmentation in case of the full proteome analyses. Only precursors with charge state 2 to 6 were selected and dynamic exclusion of 30 sec was enabled. Peptide fragmentation was performed using higher energy collision induced dissociation (HCD) and a normalized collision energy (NCE) of 26%. The precursor isolation window width was set to 1.3 m/z. MS2 Resolution was 15.000 with an automatic gain control (AGC) target value of 1e5 and maximum injection time (maxIT) of 25 msec (full proteome).

Peptide identification and quantification was performed using MaxQuant (version 1.6.3.4) with its built-in search engine Andromeda(*81*, *82*). MS2 spectra were searched against the Uniprot mus musculus proteome database (UP000000589, 54,208 protein entries, downloaded 22.3.2019) supplemented with common contaminants (built-in option in MaxQuant). Trypsin/P was specified as proteolytic enzyme. Precursor tolerance was set to 4.5 ppm, and fragment ion tolerance to 20 ppm. Results were adjusted to 1 % false discovery rate (FDR) on peptide spectrum match (PSM) level and protein level employing a target-decoy approach using reversed protein sequences. The minimal peptide length was defined as 7 amino acids, the “match-between-run” function was disabled. For full proteome analyses carbamidomethylated cysteine was

set as fixed modification and oxidation of methionine and N-terminal protein acetylation as variable modifications.

For the statistical analysis of the proteomics data, six biological replicates were measured in young and old Titan as well as young and old control mice. Protein abundances were calculated using the LFQ algorithm from MaxQuant(*83*). Before further downstream analyses, protein LFQ values were logarithm (base 10) transformed. Next, Limma (*84*) was used to identify the differentially expressed proteins between young control vs young Titan; young control vs old control; young Titan vs old Titan and old control vs old Titan. The resulted p-values were adjusted by the Benjamini-Hochberg algorithm(*85*) to control the false discovery rate (FDR). The differential analyses were performed on proteins that were identified in at least four out of six biological replicate samples in both groups under comparison.

Gene set annotations were downloaded from MSigDB(*86*), including the Gene Ontology annotation (C5 category) and pathway annotation (C2 category). The gene IDs of differentially expressed proteins were mapped to the gene set annotations. The significance of over-representation was evaluated using fisher's exact test.

Total RNA extraction for quantitative RT-PCR

RNA extraction was performed from 50mg deep frozen liver tissue. The tissue was homogenized in 1ml TRItidy G™ via pestle and incubated at room temperature for 5 minutes. After addition of 200 µl chloroform the sample was

mixed 15 seconds with the Vortex and again incubated for 2 minutes at room temperature with a following centrifugation step at 12000 x g, 4°C for 15 minutes. The aqueous phase was transferred into a new vial and mixed with 500 µl -20°C isopropanol and incubated 10 minutes at -20°C. The samples were then centrifuged at 8000 x g, 4°C for 10 minutes and the supernatant was discarded. Two washing steps with 1ml -20°C cold 70% ethanol were applied and the pellet was air-dried and dissolved in 100 µl nuclease-free water. RNA concentration was measured with NanoDrop 2000.

Quantitative Real-time PCR

A total of 800 ng RNA was used for cDNA synthesis, using the SensiFAST™cDNA Synthesis Kit (Bioline). Quantitative PCR was performed with the SensiFAST™SYBR® No-Rox Kit (Bioline) using 1.25 ng per reaction, except for the testing of mTOR (2.5 ng), and 4 pmol of forward and reverse primers. Quantitative PCR (qPCR) reactions were run on the Roche Lightcycler 96. The annealing temperature was 60°C. The qPCR data were normalized to the levels of beta-actin. Primers are listed in Table S2**.** PCR products were cleaned up using the High Pure PCR Product Purification Kit (Roche) and sequenced by LGC Genomics GmbH. Each sample was measured using two technical replicates.

Statistics and graphing

Unless stated otherwise in the RNA-seq and proteomics experimental method, statistics and graphing was conducted on GraphPad Prism 8. Unpaired two-tailed *t*-tests with Welch's correction (parametric) or MWU testing (non-parametric) were used for calculating the *P*-values unless stated otherwise. A multiple correction (FDR) was performed for SBF vs ERF qPCR and plasma analysis. A p-value ≤0.05 was used as level of significance.

Importantly, according to the GMC analysis outline, correction for multiple testing was not performed when analyzing the GMC data set (See GMC website).

Data availability

The proteomic raw data and MaxQuant search files have been deposited to the ProteomeXchange Consortium (http://proteomecentral.proteomexchange.org) via the PRIDE partner repository and can be accessed using the dataset identifier PXD019030 (reviewer account details: username reviewer73331@ebi.ac.uk; password rvqDlf58). All RNAseq data have been deposited to GEO.

Supplementary figures

Figure S1. Titan mice show early signs of impaired glucose homeostasis.

(A) Titan mice show increased levels of fasting glucose at 10-11 weeks of age. Two outliers from the Titan group were identified and removed (Values= 19.28 and 6.76). N=20 control and 17 Titan. Unpaired two-tailed *t*-tests with Welch's correction were used for calculating the *P*-values. P=0.057**.** (B) At 10-11 weeks of age, Titan mice show impaired glucose tolerance compared to control mice. N=20 control and 17 Titan. Area under the curve (AUC) t-testing P***<0.001.

Figure S2. Titan mice show signs of heart fibrosis.

H&E and Sirius Red stainings of the heart from 16-17-weeks-old control and Titan mice are shown (0.45x magnification). Sirius Red staining allows a better visualization of fibrotic tissue. Higher magnification pictures from rectangles were taken at 10x.

Figure S3. Iron levels and related binding capacity is altered in Titan mice.

Titan mice have an excess of iron in the plasma, together with low unsaturated iron binding capacity (UIBC) (p = 0.0032) and low total iron binding capacity (TIBC) (p = 0.0074) and high calculated (calc.) transferrin saturation (p = 0.0015) compared to control mice. n = 20 control vs 18 Titan for iron, N = 20 control vs 12 Titan for UIBC, TIBC and calc. transferrin saturation. ***P* < 0.01 ****P* < 0.001. Error bars indicate the SEM in all graphs. Unpaired two-tailed *t*-tests with Welch's correction were used for calculating the *P*-values.

Figure S4. Kidney H&E staining comparison of control vs Titan mice.

Representative pictures of H&E stainings of paraffin kidney tissue sections comparing 16-17-weeks old control and Titan mice. Arrows indicate basophilic tubules, tubular casts and vessel thickening in the kidneys of Titan mice. Three different magnifications are shown (0.75x, 5x and 40x).

Figure S5. Plasma electrolytes analysis show increased levels of calcium, potassium and inorganic phosphate in Titan mice.

(A-C) Titan mice show higher levels of plasma calcium, potassium and inorganic phosphate (n = 20 control vs 18 Titan). ***$P < 0.001$. Error bars indicate the SEM in all the graphs. Unpaired two-tailed *t*-tests were used for calculating the *P*-values.

Figure S6. Liver H&E staining comparison of control vs Titan mice.

Shown are representative H&E-stained images of the liver from 16-17-weeks old control and Titan mice (10x and 40x magnifications are shown). No obvious histological alterations were observed between the groups.

Figure S7. Transcriptome changes in the Liver of younger vs older Titan mice.

(A) Heat map showing significantly altered genes between 11-week-old control and Titan mice. (B) Heat map showing significantly altered genes between 11- and 19-21-week-old Titan mice. (C) GO term analysis of (B) revealed an increase in insulin-related pathway and glucose homeostasis and a decrease in various metabolic processes including fatty acid metabolism. (D) Heat map showing significantly altered genes between 19-21-week-old control and Titan mice. n=5 per group.

Figure S8. Commonly altered liver genes/proteins between control and Titan mice

Venn diagrams showing commonly regulated genes/proteins in the liver transcriptome/proteome. (A) Upregulated genes vs upregulated proteins in 11-week-old Titan mice compared to age-matched control mice. (B) Downregulated genes vs downregulated proteins in 11-week-old Titan mice compared to age-matched control mice. (C) Upregulated genes vs upregulated proteins in 19-21-week-old Titan mice compared to age-matched control mice. (D) Downregulated genes vs downregulated proteins in 19-21-week-old Titan mice compared to age-matched control mice.

Table S1. Lifespans in days days for Titan mice

Survival	Titan SBF	Titan ERF
Minimum	68	71
10% Percentile	123	214.8
25% Percentile	231.5	264
75% Percentile	405	447
90% Percentile	475	504
Maximum	614	660
Median	323.5	374
Mean	317.4	359.5
Std. Error	11.49	11.45

Table S2. Real-time PCR primer sequences.

Table S3. List of significantly altered genes

References

1. F. Bonomini, L. F. Rodella, R. Rezzani, Metabolic syndrome, aging and involvement of oxidative stress. *Aging and disease*. **6**, 109–120 (2015).

2. B. Hildrum, A. Mykletun, A. A. Dahl, K. Midthjell, Metabolic syndrome and risk of mortality in middle-aged versus elderly individuals: the Nord-Trøndelag Health Study (HUNT). *Diabetologia*. **52**, 583–590 (2009).

3. J. Lund, C. Lund, T. Morville, C. Clemmensen, The unidentified hormonal defense against weight gain. *PLoS biology*. **18**, e3000629 (2020).

4. WHO, Obesity and Overweight Factsheet (2020) (available at https://www.who.int/news-room/fact-sheets/detail/obesity-and-overweight).

5. A. J. Kennedy, K. L. J. Ellacott, V. L. King, A. H. Hasty, Mouse models of the metabolic syndrome. *Disease models & mechanisms*. **3**, 156–166 (2010).

6. S. K. Wong, K.-Y. Chin, F. H. Suhaimi, A. Fairus, S. Ima-Nirwana, Animal models of metabolic syndrome: a review. *Nutr Metabolism*. **13**, 65 (2016).

7. T. Hattori, T. Murase, M. Ohtake, T. Inoue, H. Tsukamoto, M. Takatsu, Y. Kato, K. Hashimoto, T. Murohara, K. Nagata, Characterization of a new animal model of metabolic syndrome: the DahlS.Z-Leprfa/Leprfa rat. *Nutr Diabetes*. **1**, e1–e1 (2011).

8. L. Schüler, Selection for fertility in mice - the selection plateau and how to overcome it. *TAG. Theoretical and applied genetics. Theoretische und angewandte Genetik*. **70**, 72–79 (1985).

9. G. Dietl, M. Langhammer, U. Renne, Model simulations for genetic random drift in the outbred strain Fzt:DU. *Arch Anim Breed*. **47**, 595–604 (2004).

10. L. Bünger, U. Renne, G. Dietl, S. Kuhla, Long-term selection for protein amount over 70 generations in mice. *Genetical research*. **72**, 93–109 (1998).

11. U. Renne, M. Langhammer, J. Brenmoehl, C. Walz, A. Zeissler, A. Tuchscherer, M. Piechotta, R. J. Wiesner, M. Bielohuby, A. Hoeflich, Lifelong obesity in a polygenic mouse model prevents age- and diet-induced glucose intolerance- obesity is no road to late-onset diabetes in mice. *PloS one*. **8**, e79788 (2013).

12. D. Timtchenko, J. Kratzsch, H. Sauerwein, J. Wegner, W. B. Souffrant, M. Schwerin, G. A. Brockmann, Fat storage capacity in growth-selected and control mouse lines is associated with line-specific gene expression and plasma hormone levels. *International journal of obesity and related metabolic*

disorders : journal of the International Association for the Study of Obesity. **23**, 586–594 (1999).

13. S. Aksu, D. Koczan, U. Renne, H.-J. Thiesen, G. A. Brockmann, Differentially expressed genes in adipose tissues of high body weight-selected (obese) and unselected (lean) mouse lines. *Journal of applied genetics*. **48**, 133–143 (2007).

14. J. Brenmoehl, C. Walz, M. Spitschak, E. Wirthgen, M. Walz, M. Langhammer, A. Tuchscherer, R. Naumann, A. Hoeflich, Partial phenotype conversion and differential trait response to conditions of husbandry in mice. *J Comp Physiology B*. **188**, 527–539 (2018).

15. C. Selman, D. H. Nussey, P. Monaghan, Ageing: it's a dog's life. *Current biology : CB*. **23**, R451-3 (2013).

16. M. Walz, L. Chau, C. Walz, M. Sawitzky, D. Ohde, J. Brenmoehl, A. Tuchscherer, M. Langhammer, F. Metzger, C. Höflich, A. Hoeflich, Overlap of Peak Growth Activity and Peak IGF-1 to IGFBP Ratio: Delayed Increase of IGFBPs Versus IGF-1 in Serum as a Mechanism to Speed up and down Postnatal Weight Gain in Mice. *Cells*. **9**, 1516 (2020).

17. I. Shimizu, K. Walsh, The Whitening of Brown Fat and Its Implications for Weight Management in Obesity. *Curr Obes Reports*. **4**, 224–229 (2015).

18. R. Catanzaro, B. Cuffari, A. Italia, F. Marotta, Exploring the metabolic syndrome: Nonalcoholic fatty pancreas disease. *World journal of gastroenterology*. **22**, 7660–7675 (2016).

19. A. Guilherme, F. Henriques, A. H. Bedard, M. P. Czech, Molecular pathways linking adipose innervation to insulin action in obesity and diabetes mellitus. *Nature reviews. Endocrinology*. **15**, 207–225 (2019).

20. X. Zhang, D. C. Y. Yeung, M. Karpisek, D. Stejskal, Z.-G. Zhou, F. Liu, R. L. C. Wong, W.-S. Chow, A. W. K. Tso, K. S. L. Lam, A. Xu, Serum FGF21 levels are increased in obesity and are independently associated with the metabolic syndrome in humans. *Diabetes*. **57**, 1246–1253 (2008).

21. M. Giralt, A. Gavaldà-Navarro, F. Villarroya, Fibroblast growth factor-21, energy balance and obesity. *Mol Cell Endocrinol*. **418**, 66–73 (2015).

22. L. Y. Chen, S. D. Chang, G. M. Sreenivasan, P. W. Tsang, R. C. Broady, C. H. Li, L. N. Zypchen, Dysmetabolic hyperferritinemia is associated with normal transferrin saturation, mild hepatic iron overload, and elevated hepcidin. *Annals of hematology*. **90**, 139–143 (2011).

23. H. Senjo, T. Higuchi, S. Okada, O. Takahashi, Hyperferritinemia: causes and significance in a general hospital. *Hematology (Amsterdam, Netherlands)*. **23**, 817–822 (2018).

24. R. Monteiro, I. Azevedo, Chronic inflammation in obesity and the metabolic syndrome. *Mediators of inflammation*. **2010** (2010), doi:10.1155/2010/289645.

25. J. M. Ward, J. E. Rehg, H. C. Morse, Differentiation of rodent immune and hematopoietic system reactive lesions from neoplasias. *Toxicologic pathology*. **40**, 425–434 (2012).

26. C. P. Kovesdy, S. L. Furth, C. Zoccali, W. K. D. S. Committee, Obesity and Kidney Disease. *Can J Kidney Heal Dis*. **4**, 2054358117698669 (2017).

27. J. E. Hall, J. M. do Carmo, A. A. da Silva, Z. Wang, M. E. Hall, Obesity, kidney dysfunction and hypertension: mechanistic links. *Nat Rev Nephrol*. **15**, 367–385 (2019).

28. A. R. Khan, F. R. Awan, S. S. Najam, M. Islam, T. Siddique, M. Zain, Elevated serum level of human alkaline phosphatase in obesity. *Jpma J Pak Medical Assoc*. **65**, 1182–5 (2015).

29. E. G. Giannini, R. Testa, V. Savarino, Liver enzyme alteration: a guide for clinicians. *Can Med Assoc J*. **172**, 367–379 (2005).

30. A. A. Toye, M. E. Dumas, C. Blancher, A. R. Rothwell, J. F. Fearnside, S. P. Wilder, M. T. Bihoreau, O. Cloarec, I. Azzouzi, S. Young, R. H. Barton, E. Holmes, M. I. McCarthy, R. Tatoud, J. K. Nicholson, J. Scott, D. Gauguier, Subtle metabolic and liver gene transcriptional changes underlie diet-induced fatty liver susceptibility in insulin-resistant mice. *Diabetologia*. **50**, 1867–1879 (2007).

31. D. F. V. Lewis, 57 varieties: the human cytochromes P450. *Pharmacogenomics*. **5**, 305–318 (2004).

32. E. T. Morgan, Impact of infectious and inflammatory disease on cytochrome P450-mediated drug metabolism and pharmacokinetics. *Clinical pharmacology and therapeutics*. **85**, 434–438 (2009).

33. E. Siewert, R. Bort, R. Kluge, P. C. Heinrich, J. Castell, R. Jover, Hepatic cytochrome P450 down-regulation during aseptic inflammation in the mouse is interleukin 6 dependent. *Hepatology (Baltimore, Md.)*. **32**, 49–55 (2000).

34. T. Maier, M. Güell, L. Serrano, Correlation of mRNA and protein in complex biological samples. *FEBS letters*. **583**, 3966–3973 (2009).

35. M. J. Wilkinson, E. N. C. Manoogian, A. Zadourian, H. Lo, S. Fakhouri, A. Shoghi, X. Wang, J. G. Fleischer, S. Navlakha, S. Panda, P. R. Taub, Ten-Hour Time-Restricted Eating Reduces Weight, Blood Pressure, and Atherogenic Lipids in Patients with Metabolic Syndrome. *Cell Metab*. **31**, 92-104.e5 (2019).

36. L. Fontana, L. Partridge, Promoting health and longevity through diet: from model organisms to humans. *Cell*. **161**, 106–118 (2015).

37. A. D. Francesco, C. D. Germanio, M. Bernier, R. de Cabo, A time to fast. *Science (New York, N.Y.)*. **362**, 770–775 (2018).

38. E. L. Greer, A. Brunet, Different dietary restriction regimens extend lifespan by both independent and overlapping genetic pathways in C. elegans. *Aging cell*. **8**, 113–127 (2009).

39. H. Li, J. Auwerx, Mouse Systems Genetics as a Prelude to Precision Medicine. *Trends in genetics : TIG* (2020), doi:10.1016/j.tig.2020.01.004.

40. C.-Y. Liao, B. A. Rikke, T. E. Johnson, V. Diaz, J. F. Nelson, Genetic variation in the murine lifespan response to dietary restriction: from life extension to life shortening. *Aging cell*. **9**, 92–95 (2010).

41. Y. Mahendran, H. Cederberg, J. Vangipurapu, A. J. Kangas, P. Soininen, J. Kuusisto, M. Uusitupa, M. Ala-Korpela, M. Laakso, Glycerol and Fatty Acids in Serum Predict the Development of Hyperglycemia and Type 2 Diabetes in Finnish Men. *Diabetes Care*. **36**, 3732–3738 (2013).

42. F. Karpe, J. R. Dickmann, K. N. Frayn, Fatty Acids, Obesity, and Insulin Resistance: Time for a Reevaluation. *Diabetes*. **60**, 2441–2449 (2011).

43. S. M. Grundy, J. I. Cleeman, S. R. Daniels, K. A. Donato, R. H. Eckel, B. A. Franklin, D. J. Gordon, R. M. Krauss, P. J. Savage, S. C. Smith, J. A. Spertus, F. Costa, Diagnosis and management of the metabolic syndrome: an American Heart Association/National Heart, Lung, and Blood Institute scientific statement: Executive Summary. *Critical pathways in cardiology*. **4**, 198–203 (2005).

44. M. N. B. Kristiansen, S. S. Veidal, K. T. G. Rigbolt, K. S. Tølbøl, J. D. Roth, J. Jelsing, N. Vrang, M. Feigh, Obese diet-induced mouse models of nonalcoholic steatohepatitis-tracking disease by liver biopsy. *World J Hepatology*. **8**, 673–684 (2016).

45. J. M. Gallego-Escuredo, J. Gómez-Ambrosi, V. Catalan, P. Domingo, M. Giralt, G. Frühbeck, F. Villarroya, Opposite alterations in FGF21 and FGF19 levels and disturbed expression of the receptor machinery for endocrine FGFs in obese patients. *Int J Obesity*. **39**, 121–129 (2015).

46. J. Díaz-Delfín, E. Hondares, R. Iglesias, M. Giralt, C. Caelles, F. Villarroya, TNF-α Represses β-Klotho Expression and Impairs FGF21 Action in Adipose Cells: Involvement of JNK1 in the FGF21 Pathway. *Endocrinology*. **153**, 4238–4245 (2012).

47. R. Pezzilli, L. Calculli, Pancreatic steatosis: Is it related to either obesity or diabetes mellitus? *World J Diabetes*. **5**, 415 (2014).

48. K. E. Pinnick, S. C. Collins, C. Londos, D. Gauguier, A. Clark, B. A. Fielding, Pancreatic Ectopic Fat Is Characterized by Adipocyte Infiltration and Altered Lipid Composition. *Obesity*. **16**, 522–530 (2008).

49. M. Cavalera, J. Wang, N. G. Frangogiannis, Obesity, metabolic dysfunction, and cardiac fibrosis: pathophysiological pathways, molecular mechanisms, and therapeutic opportunities. *Transl Res*. **164**, 323–335 (2014).

50. P. Bao, G. Liu, Y. Wei, Association between IL-6 and related risk factors of metabolic syndrome and cardiovascular disease in young rats. *International journal of clinical and experimental medicine*. **8**, 13491–13499 (2015).

51. A. D. Pradhan, J. E. Manson, N. Rifai, J. E. Buring, P. M. Ridker, C-reactive protein, interleukin 6, and risk of developing type 2 diabetes mellitus. *JAMA*. **286**, 327–334 (2001).

52. M. Mohammadi, M. H. Gozashti, M. Aghadavood, M. R. Mehdizadeh, M. M. Hayatbakhsh, Clinical Significance of Serum IL-6 and TNF-α Levels in Patients with Metabolic Syndrome. *Reports of biochemistry & molecular biology*. **6**, 74–79 (2017).

53. P. C. Heinrich, I. Behrmann, S. Haan, H. M. Hermanns, G. Müller-Newen, F. Schaper, Principles of interleukin (IL)-6-type cytokine signalling and its regulation. *The Biochemical journal*. **374**, 1–20 (2003).

54. G. Landskron, M. D. la Fuente, P. Thuwajit, C. Thuwajit, M. A. Hermoso, Chronic inflammation and cytokines in the tumor microenvironment. *Journal of immunology research*. **2014**, 149185 (2014).

55. K. Popko, E. Gorska, A. Stelmaszczyk-Emmel, R. Plywaczewski, A. Stoklosa, D. Gorecka, B. Pyrzak, U. Demkow, Proinflammatory cytokines Il-6 and TNF-α and the development of inflammation in obese subjects. *European journal of medical research*. **15 Suppl 2**, 120–122 (2010).

56. J. H. Lee, Y. E. Kang, J. Y. Chang, K. C. Park, H.-W. Kim, J. T. Kim, H. J. Kim, H.-S. Yi, M. Shong, H. K. Chung, K. S. Kim, An engineered FGF21 variant, LY2405319, can prevent non-alcoholic steatohepatitis by enhancing hepatic mitochondrial function. *Am J Transl Res*. **8**, 4750–4763 (2016).

57. H. Morinaga, R. Mayoral, J. Heinrichsdorff, O. Osborn, N. Franck, N. Hah, E. Walenta, G. Bandyopadhyay, A. R. Pessentheiner, T. J. Chi, H. Chung, J. G. Bogner-Strauss, R. M. Evans, J. M. Olefsky, D. Y. Oh, Characterization of Distinct Subpopulations of Hepatic Macrophages in HFD/Obese Mice. *Diabetes*. **64**, 1120–1130 (2014).

58. S. P. Weisberg, D. McCann, M. Desai, M. Rosenbaum, R. L. Leibel, A. W. Ferrante, Obesity is associated with macrophage accumulation in adipose tissue. *J Clin Invest*. **112**, 1796–1808 (2003).

59. S. Sun, Y. Ji, S. Kersten, L. Qi, Mechanisms of Inflammatory Responses in Obese Adipose Tissue. *Annu Rev Nutr*. **32**, 261–286 (2012).

60. M. Ito, J. Suzuki, S. Tsujioka, M. Sasaki, A. Gomori, T. Shirakura, H. Hirose, M. Ito, A. Ishihara, H. Iwaasa, A. Kanatani, Longitudinal analysis of murine

steatohepatitis model induced by chronic exposure to high-fat diet. *Hepatol Res*. **37**, 50–57 (2007).

61. H. M. Ayoub, M. R. McDonald, J. A. Sullivan, R. Tsao, K. A. Meckling, Proteomic Profiles of Adipose and Liver Tissues from an Animal Model of Metabolic Syndrome Fed Purple Vegetables. *Nutrients*. **10** (2018), doi:10.3390/nu10040456.

62. C.-C. Hsieh, C.-C. Liao, Y.-C. Liao, L. S. Hwang, L.-Y. Wu, S.-C. Hsieh, Proteomic changes associated with metabolic syndrome in a fructose-fed rat model. *Journal of food and drug analysis*. **24**, 754–761 (2016).

63. P. Crocco, A. Montesanto, S. Dato, S. Geracitano, F. Iannone, G. Passarino, G. Rose, Inter-Individual Variability in Xenobiotic-Metabolizing Enzymes: Implications for Human Aging and Longevity. *Genes*. **10** (2019), doi:10.3390/genes10050403.

64. M. W. Chou, J. Kong, K. T. Chung, R. W. Hart, Effect of caloric restriction on the metabolic activation of xenobiotics. *Mutation research*. **295**, 223–235 (1993).

65. C. Hine, E. Harputlugil, Y. Zhang, C. Ruckenstuhl, B. C. Lee, L. Brace, A. Longchamp, J. H. Treviño-Villarreal, P. Mejia, C. K. Ozaki, R. Wang, V. N. Gladyshev, F. Madeo, W. B. Mair, J. R. Mitchell, Endogenous hydrogen sulfide production is essential for dietary restriction benefits. *Cell*. **160**, 132–144 (2015).

66. F. Obata, M. Miura, Enhancing S-adenosyl-methionine catabolism extends Drosophila lifespan. *Nature communications*. **6**, 8332 (2015).

67. F. Obata, E. Kuranaga, K. Tomioka, M. Ming, A. Takeishi, C.-H. Chen, T. Soga, M. Miura, Necrosis-driven systemic immune response alters SAM metabolism through the FOXO-GNMT axis. *Cell reports*. **7**, 821–833 (2014).

68. S. M. Poiley, A systematic method of breeder rotation for non-inbred laboratory animal colonies. *Proc Anim Care Panel*, 159–166 (1960).

69. T. H. Meuwissen, Maximizing the response of selection with a predefined rate of inbreeding. *Journal of animal science*. **75**, 934–940 (1997).

70. V. Gailus-Durner, H. Fuchs, L. Becker, I. Bolle, M. Brielmeier, J. Calzada-Wack, R. Elvert, N. Ehrhardt, C. Dalke, T. J. Franz, E. Grundner-Culemann, S. Hammelbacher, S. M. Hölter, G. Hölzlwimmer, M. Horsch, A. Javaheri, S. V. Kalaydjiev, M. Klempt, E. Kling, S. Kunder, C. Lengger, T. Lisse, T. Mijalski, B. Naton, V. Pedersen, C. Prehn, G. Przemeck, I. Racz, C. Reinhard, P. Reitmeir, I. Schneider, A. Schrewe, R. Steinkamp, C. Zybill, J. Adamski, J. Beckers, H. Behrendt, J. Favor, J. Graw, G. Heldmaier, H. Höfler, B. Ivandic, H. Katus, P. Kirchhof, M. Klingenspor, T. Klopstock, A. Lengeling, W. Müller, F. Ohl, M. Ollert, L. Quintanilla-Martinez, J. Schmidt, H. Schulz, E. Wolf, W. Wurst, A. Zimmer, D. H. Busch, M. H. de Angelis, Introducing the German Mouse Clinic:

open access platform for standardized phenotyping. *Nature methods*. **2**, 403–404 (2005).

71. H. Fuchs, V. Gailus-Durner, T. Adler, J. A. Aguilar-Pimentel, L. Becker, J. Calzada-Wack, P. D. Silva-Buttkus, F. Neff, A. Götz, W. Hans, S. M. Hölter, M. Horsch, G. Kastenmüller, E. Kemter, C. Lengger, H. Maier, M. Matloka, G. Möller, B. Naton, C. Prehn, O. Puk, I. Racz, B. Rathkolb, W. Römisch-Margl, J. Rozman, R. Wang-Sattler, A. Schrewe, C. Stöger, M. Tost, J. Adamski, B. Aigner, J. Beckers, H. Behrendt, D. H. Busch, I. Esposito, J. Graw, T. Illig, B. Ivandic, M. Klingenspor, T. Klopstock, E. Kremmer, M. Mempel, S. Neschen, M. Ollert, H. Schulz, K. Suhre, E. Wolf, W. Wurst, A. Zimmer, M. H. de Angelis, Mouse phenotyping. *Methods (San Diego, Calif.)*. **53**, 120–135 (2011).

72. B. Rathkolb, W. Hans, C. Prehn, H. Fuchs, V. Gailus-Durner, B. Aigner, J. Adamski, E. Wolf, M. H. de Angelis, Clinical Chemistry and Other Laboratory Tests on Mouse Plasma or Serum. *Current protocols in mouse biology*. **3**, 69–100 (2013).

73. J. Rozman, B. Rathkolb, S. Neschen, H. Fuchs, V. Gailus-Durner, M. Klingenspor, E. Wolf, M. H. de Angelis, Glucose tolerance tests for systematic screening of glucose homeostasis in mice. *Current protocols in mouse biology*. **5**, 65–84 (2015).

74. A. Dobin, T. R. Gingeras, *Current protocols in bioinformatics*, in press, doi:10.1002/0471250953.bi1114s51.

75. M. I. Love, W. Huber, S. Anders, Moderated estimation of fold change and dispersion for RNA-seq data with DESeq2. *Genome biology*. **15**, 550 (2014).

76. G. Yu, L.-G. Wang, Y. Han, Q.-Y. He, clusterProfiler: an R package for comparing biological themes among gene clusters. *Omics : a journal of integrative biology*. **16**, 284–287 (2012).

77. H. Wickham, ggplot2, Elegant Graphics for Data Analysis, 147–168 (2016).

78. H. Chen, P. C. Boutros, VennDiagram: a package for the generation of highly-customizable Venn and Euler diagrams in R. *BMC bioinformatics*. **12**, 35 (2011).

79. J. Gaucher, K. Kinouchi, N. Ceglia, E. Montellier, S. Peleg, C. M. Greco, A. Schmidt, I. Forne, S. Masri, P. Baldi, A. Imhof, P. Sassone-Corsi, Distinct metabolic adaptation of liver circadian pathways to acute and chronic patterns of alcohol intake. *Proceedings of the National Academy of Sciences of the United States of America*. **116**, 25250–25259 (2019).

80. S. Peleg, C. Feller, I. Forne, E. Schiller, D. C. Sévin, T. Schauer, C. Regnard, T. Straub, M. Prestel, C. Klima, M. S. Nogueira, L. Becker, T. Klopstock, U. Sauer, P. B. Becker, A. Imhof, A. G. Ladurner, Life span

extension by targeting a link between metabolism and histone acetylation in Drosophila. *EMBO reports*. **17**, 455–469 (2016).

81. J. Cox, N. Neuhauser, A. Michalski, R. A. Scheltema, J. V. Olsen, M. Mann, Andromeda: a peptide search engine integrated into the MaxQuant environment. *Journal of proteome research*. **10**, 1794–1805 (2011).

82. S. Tyanova, T. Temu, J. Cox, The MaxQuant computational platform for mass spectrometry-based shotgun proteomics. *Nature protocols*. **11**, 2301–2319 (2016).

83. J. Cox, M. Y. Hein, C. A. Luber, I. Paron, N. Nagaraj, M. Mann, Accurate proteome-wide label-free quantification by delayed normalization and maximal peptide ratio extraction, termed MaxLFQ. *Molecular & cellular proteomics : MCP*. **13**, 2513–2526 (2014).

84. M. E. Ritchie, B. Phipson, D. Wu, Y. Hu, C. W. Law, W. Shi, G. K. Smyth, limma powers differential expression analyses for RNA-sequencing and microarray studies. *Nucleic acids research*. **43**, e47 (2015).

85. Y. Benjamini, Y. Hochberg, Controlling the False Discovery Rate: A Practical and Powerful Approach to Multiple Testing. *Journal of the Royal Statistical Society*. **57**, 289–300 (1995).

86. A. Liberzon, C. Birger, H. Thorvaldsdóttir, M. Ghandi, J. P. Mesirov, P. Tamayo, The Molecular Signatures Database (MSigDB) hallmark gene set collection. *Cell systems*. **1**, 417–425 (2015).

Figure 1

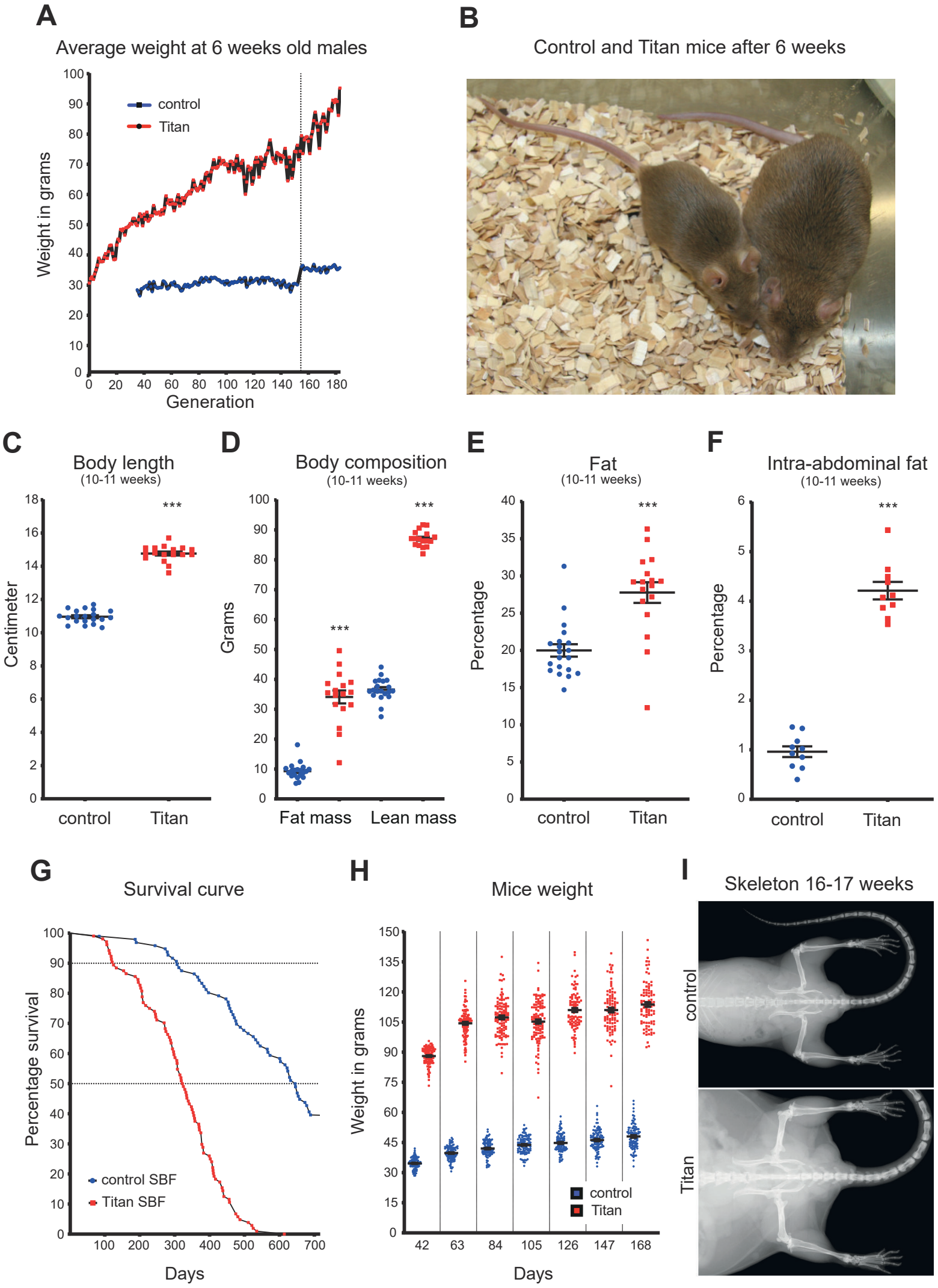
A
Average weight at 6 weeks old males
control
Titan
Weight in grams
Generation
B
Control and Titan mice after 6 weeks
C
Body length
(10-11 weeks)
Centimeter
control
Titan
D
Body composition
(10-11 weeks)
Grams
Fat mass
Lean mass
E
Fat
(10-11 weeks)
Percentage
control
Titan
F
Intra-abdominal fat
(10-11 weeks)
Percentage
control
Titan
G
Survival curve
Percentage survival
control SBF
Titan SBF
Days
H
Mice weight
Weight in grams
control
Titan
Days
I
Skeleton 16-17 weeks
control
Titan

Figure 2

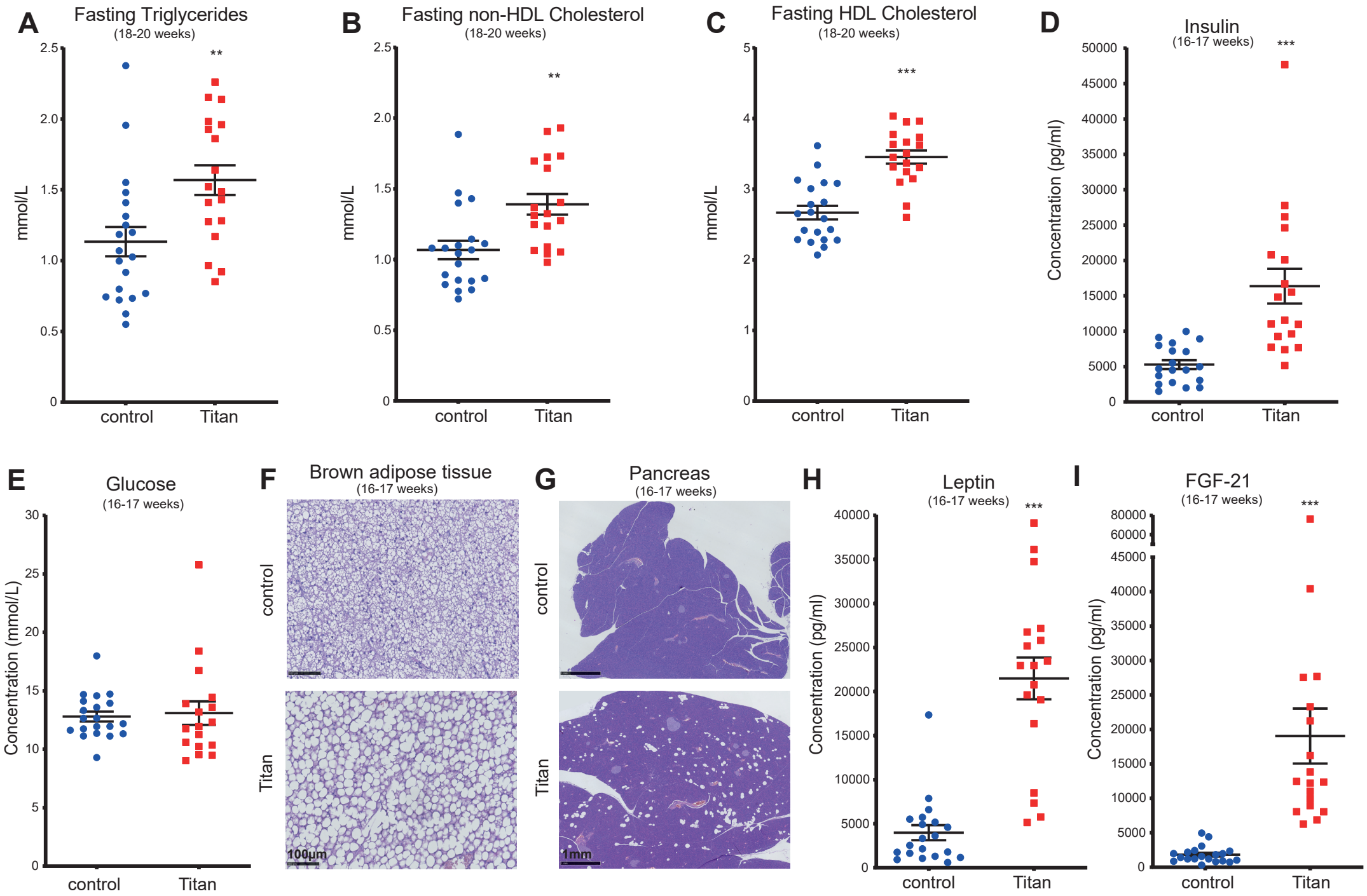
A
Fasting Triglycerides
(18-20 weeks)
mmol/L
control
Titan
B
Fasting non-HDL Cholesterol
(18-20 weeks)
mmol/L
control
Titan
C
Fasting HDL Cholesterol
(18-20 weeks)
mmol/L
control
Titan
D
Insulin
(16-17 weeks)
Concentration (pg/ml)
control
Titan
E
Glucose
(16-17 weeks)
Concentration (mmol/L)
control
Titan
F
Brown adipose tissue
(16-17 weeks)
control
Titan
100µm
G
Pancreas
(16-17 weeks)
control
Titan
1mm
H
Leptin
(16-17 weeks)
Concentration (pg/ml)
control
Titan
I
FGF-21
(16-17 weeks)
Concentration (pg/ml)
control
Titan

Figure 3

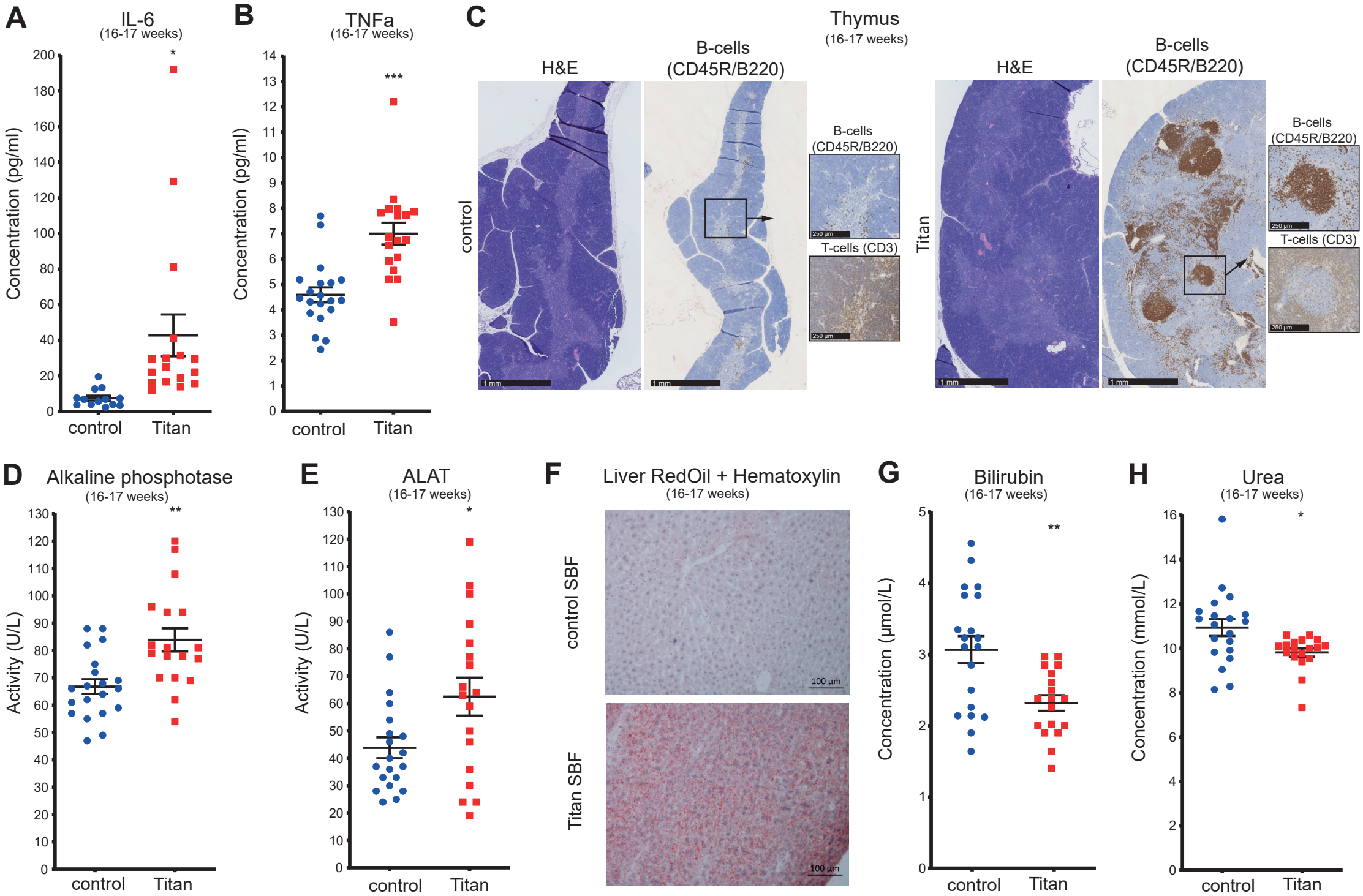
A
IL-6
(16-17 weeks)
Concentration (pg/ml)
control
Titan
B
TNFa
(16-17 weeks)
Concentration (pg/ml)
control
Titan
C
Thymus
(16-17 weeks)
H&E
B-cells
(CD45R/B220)
T-cells (CD3)
control
Titan
D
Alkaline phosphotase
(16-17 weeks)
Activity (U/L)
control
Titan
E
ALAT
(16-17 weeks)
Activity (U/L)
control
Titan
F
Liver RedOil + Hematoxylin
(16-17 weeks)
control SBF
Titan SBF
G
Bilirubin
(16-17 weeks)
Concentration (µmol/L)
control
Titan
H
Urea
(16-17 weeks)
Concentration (mmol/L)
control
Titan

Figure 4

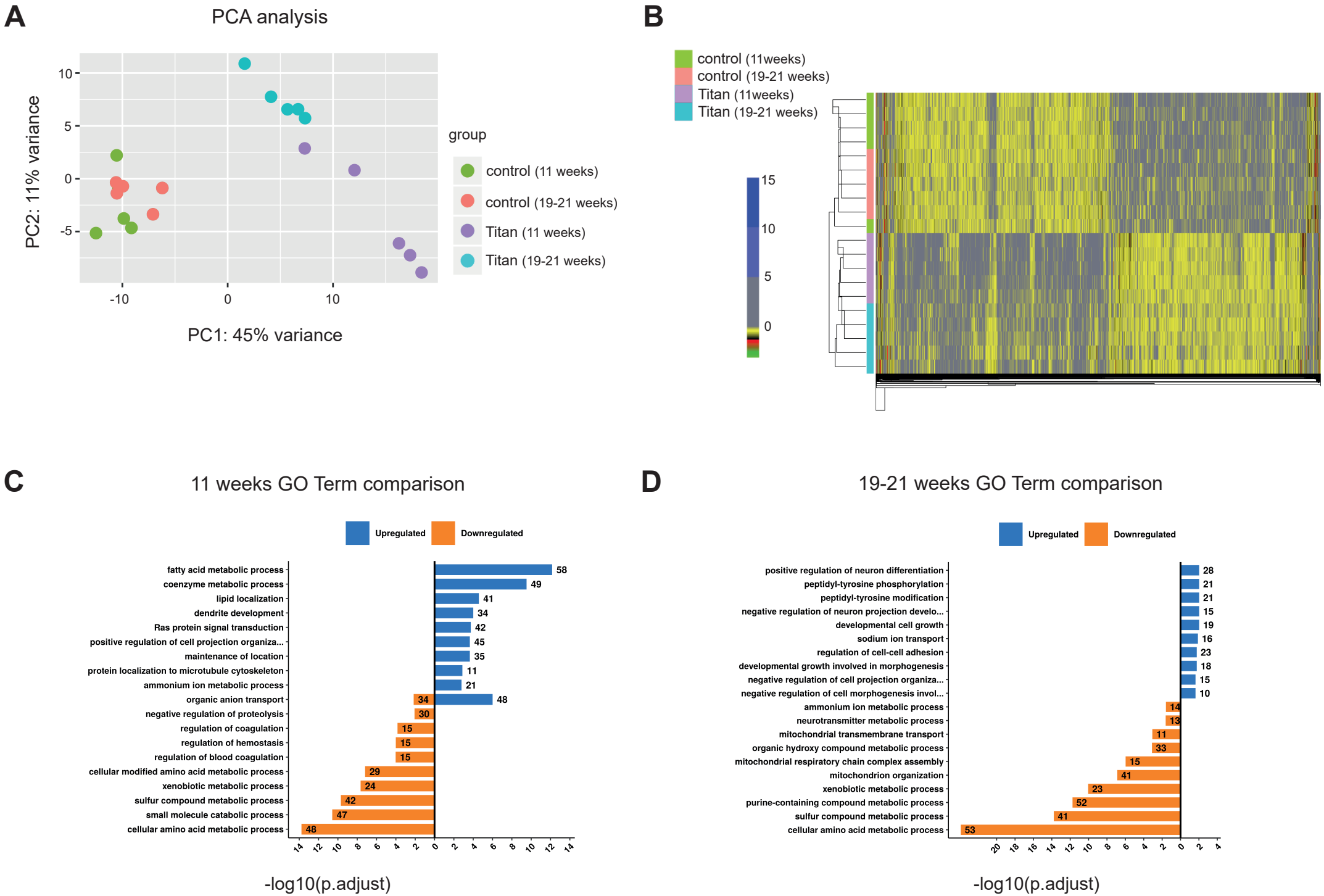
A
PCA analysis
PC2: 11% variance
PC1: 45% variance
10
5
0
-5
-10
0
10
group
control (11 weeks)
control (19-21 weeks)
Titan (11 weeks)
Titan (19-21 weeks)
B
control (11weeks)
control (19-21 weeks)
Titan (11weeks)
Titan (19-21 weeks)
15
10
5
0
C
11 weeks GO Term comparison
Upregulated
Downregulated
fatty acid metabolic process 58
coenzyme metabolic process 49
lipid localization 41
dendrite development 34
Ras protein signal transduction 42
positive regulation of cell projection organiza... 45
maintenance of location 35
protein localization to microtubule cytoskeleton 11
ammonium ion metabolic process 21
organic anion transport 34 48
negative regulation of proteolysis 30
regulation of coagulation 15
regulation of hemostasis 15
regulation of blood coagulation 15
cellular modified amino acid metabolic process 29
xenobiotic metabolic process 24
sulfur compound metabolic process 42
small molecule catabolic process 47
cellular amino acid metabolic process 48
14 12 10 8 6 4 2 0 2 4 6 8 10 12 14
-log10(p.adjust)
D
19-21 weeks GO Term comparison
Upregulated
Downregulated
positive regulation of neuron differentiation 28
peptidyl-tyrosine phosphorylation 21
peptidyl-tyrosine modification 21
negative regulation of neuron projection develo... 15
developmental cell growth 19
sodium ion transport 16
regulation of cell-cell adhesion 23
developmental growth involved in morphogenesis 18
negative regulation of cell projection organiza... 15
negative regulation of cell morphogenesis invol... 10
ammonium ion metabolic process 14
neurotransmitter metabolic process 13
mitochondrial transmembrane transport 11
organic hydroxy compound metabolic process 33
mitochondrial respiratory chain complex assembly 15
mitochondrion organization 41
xenobiotic metabolic process 23
purine-containing compound metabolic process 52
sulfur compound metabolic process 41
cellular amino acid metabolic process 53
20 18 16 14 12 10 8 6 4 2 0 2 4
-log10(p.adjust)

Figure 5

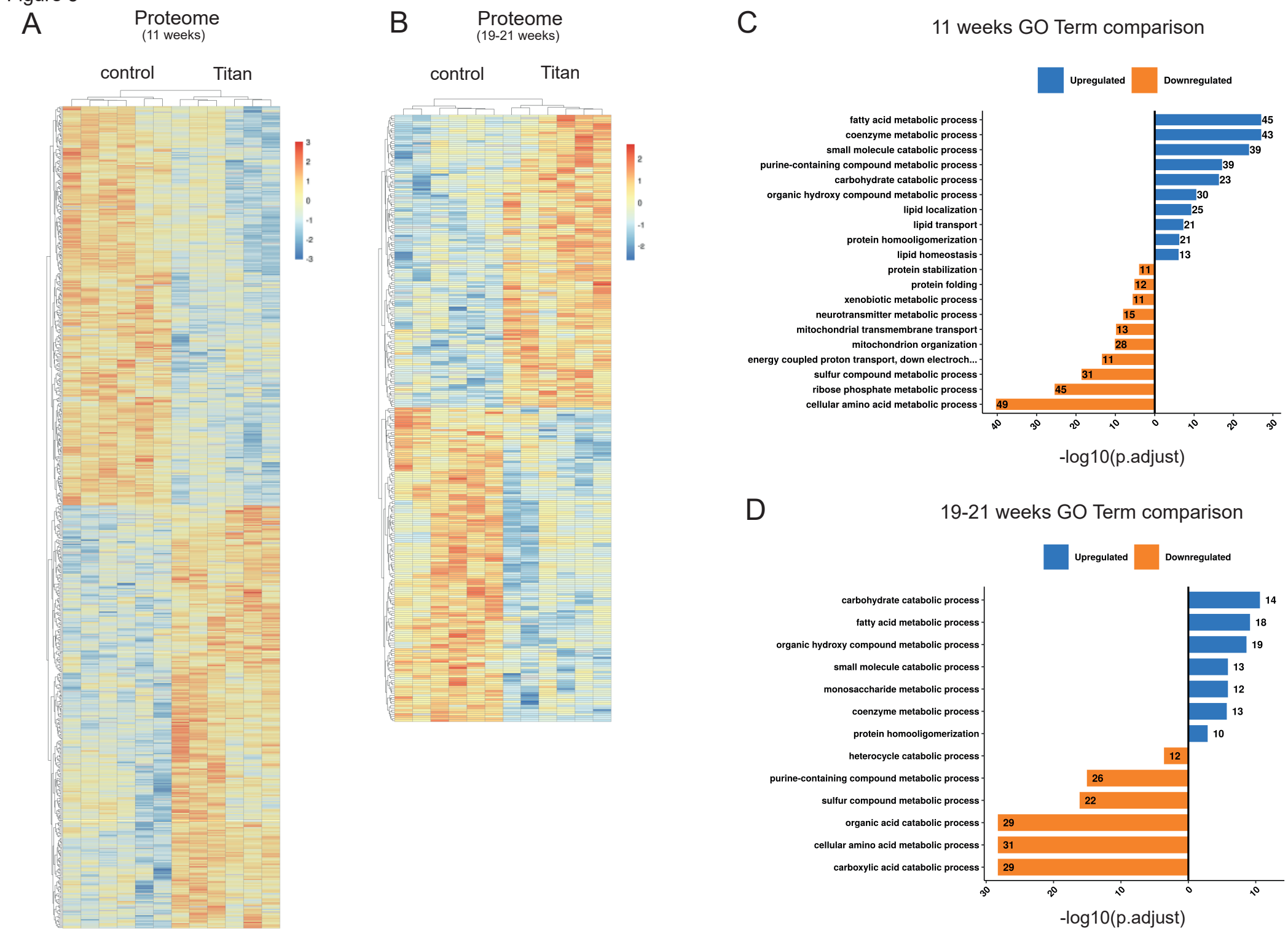
A
Proteome
(11 weeks)
control
Titan
3
2
1
0
-1
-2
-3
B
Proteome
(19-21 weeks)
control
Titan
2
1
0
-1
-2
C
11 weeks GO Term comparison
Upregulated
Downregulated
fatty acid metabolic process 45
coenzyme metabolic process 43
small molecule catabolic process 39
purine-containing compound metabolic process 39
carbohydrate catabolic process 23
organic hydroxy compound metabolic process 30
lipid localization 25
lipid transport 21
protein homooligomerization 21
lipid homeostasis 13
protein stabilization 11
protein folding 12
xenobiotic metabolic process 11
neurotransmitter metabolic process 15
mitochondrial transmembrane transport 13
mitochondrion organization 28
energy coupled proton transport, down electroch... 11
sulfur compound metabolic process 31
ribose phosphate metabolic process 45
cellular amino acid metabolic process 49
40 30 20 10 0 10 20 30
-log10(p.adjust)
D
19-21 weeks GO Term comparison
Upregulated
Downregulated
carbohydrate catabolic process 14
fatty acid metabolic process 18
organic hydroxy compound metabolic process 19
small molecule catabolic process 13
monosaccharide metabolic process 12
coenzyme metabolic process 13
protein homooligomerization 10
heterocycle catabolic process 12
purine-containing compound metabolic process 26
sulfur compound metabolic process 22
organic acid catabolic process 29
cellular amino acid metabolic process 31
carboxylic acid catabolic process 29
30 20 10 0 10
-log10(p.adjust)

Figure 6

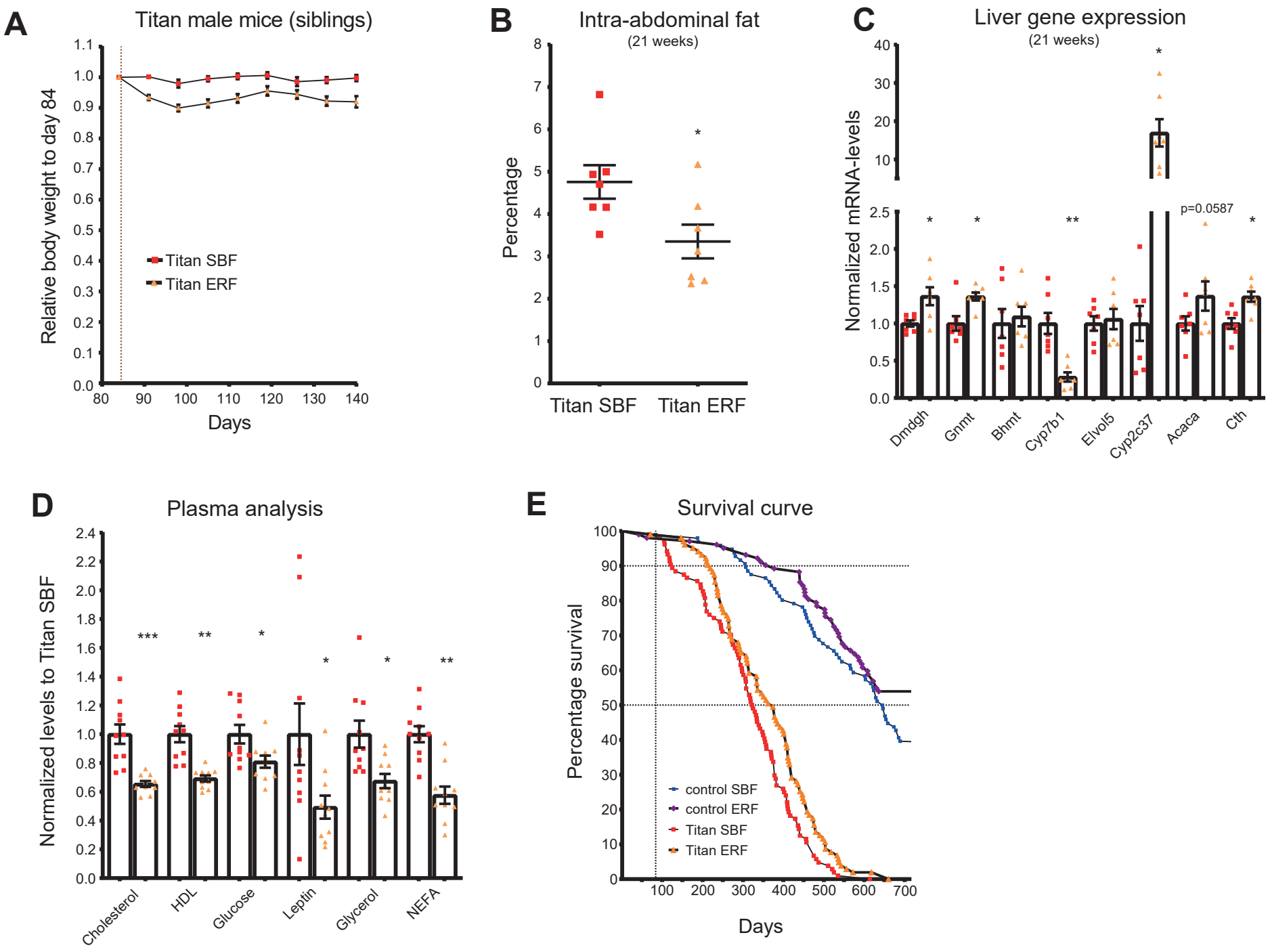
A
Titan male mice (siblings)
Relative body weight to day 84
Days
Titan SBF
Titan ERF
B
Intra-abdominal fat
(21 weeks)
Percentage
Titan SBF
Titan ERF
C
Liver gene expression
(21 weeks)
Normalized mRNA-levels
p=0.0587
Dmdgh
Gnmt
Bhmt
Cyp7b1
Elvol5
Cyp2c37
Acaca
Cth
D
Plasma analysis
Normalized levels to Titan SBF
Cholesterol
HDL
Glucose
Leptin
Glycerol
NEFA
E
Survival curve
Percentage survival
control SBF
control ERF
Titan SBF
Titan ERF
Days